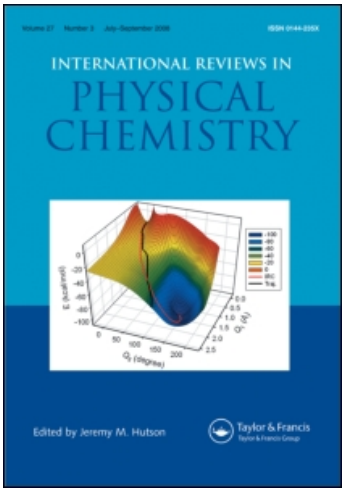

International Reviews in Physical Chemistry
Publication details, including instructions for authors and subscription information:
http://www.informaworld.com/smpp/title~content=t713724383

Progress in computer simulations of liquid crystals

Mark R. Wilson[a]
[a] Department of Chemistry, University of Durham, Science Laboratories, Durham

To cite this Article Wilson, Mark R.(2005) 'Progress in computer simulations of liquid crystals', International Reviews in Physical Chemistry, 24: 3, 421 — 455
To link to this Article: DOI: 10.1080/01442350500361244
URL: http://dx.doi.org/10.1080/01442350500361244

International Reviews in Physical Chemistry,
Vol. 24, Nos. 3–4, July–December 2005, 421–455

Taylor & Francis
Taylor & Francis Group

Progress in computer simulations of liquid crystals

MARK R. WILSON*

Department of Chemistry, University of Durham,
Science Laboratories, South Road, Durham, DH1 3LE

(*Received 04 October 2005; in final form 15 September 2005*)

This article reviews some of the recent progress in the simulation of liquid crystals across a range of length and time scales. Simulators now have an extensive range of models at their disposal, ranging from fully atomistic studies where each atom is represented in a simulation, via hard or soft anisotropic potentials, to lattice models and director-based simulation methods. Each of these provide access to different phenomena. The progress towards accurate atomistic modelling of nematics is discussed in detail, pointing to improvements in force fields made recently and discussing the progress towards accurate prediction of material properties. Three material properties are discussed in detail: elastic constants, rotational viscosity and helical twisting powers. The simulation methods that can be employed to extract such properties are reviewed and the insights provided by recent results from atomistic and coarse-grained models are discussed. The article points also to the recent success of coarse-grained modelling in helping to understand the structure of complex macromolecular liquid crystals: liquid crystal polymers and liquid crystal dendrimers in which the macromolecules contain different types of interaction site. Finally, it is worth noting that throughout Nature liquid crystals occur as the archetypal self-assembled materials; able to form well-defined self-organized structures, which are often ordered at the nanoscale. With this in mind, some perspectives on the future use of these materials are presented, with suggestions for how liquid crystal simulation can be used to help in the design of the next generation of nanoscale devices.

Contents

*Email: mark.wilson@durham.ac.uk

International Reviews in Physical Chemistry
ISSN 0144–235X print/ISSN 1366–591X online
http://www.tandf.co.uk/journals
DOI: 10.1080/01442350500361244

1. Introduction

Liquid crystals are the quintessential soft self-organizing molecular materials. They are able to form anisotropic structures with bulk material and electronic properties that are directional, while simultaneously retaining many characteristics that are more akin to fluids. This combination of properties from both the crystal and liquid regimes have led to interesting applications, which arise (in many cases) from the ability of liquid crystals to *switch* in response to external stimuli. Most ubiquitous of these is the role played by liquid crystal displays (LCDs), which have infiltrated most aspects of modern life from wrist-watches to computer screens [1]. Less well known are uses of liquid crystals as colour-tunable lasers [2–4], as sensitive temperature sensors in medical applications and non-destructive testing, as functional polymers [5, 6], as materials for adaptive optics [7, 8], and as phase modulators in optical telecommunications [9, 10]. More intriguing still are the possible applications of liquid crystalline materials in the next generation of self-assembled photonic nanostructures [11] and in a new generation of materials for biomimetic applications [12].

Basic liquid crystal theory is well established. The idea of a simple molecular mean field theory for the nematic–isotropic transition was developed by Maier and Saupe in the 1950s based on the idea of anisotropic dispersion forces [13]. The Maier–Saupe approach works well in explaining the temperature dependence of nematic order and the weakly first-order nature of the nematic–isotropic phase transition for thermotropic LC materials. Prior to this, in the 1940s, Onsager was able to show that rigid rod particles should undergo a transition from an isotropic to a nematic phase as a function of density [14], thus providing a basis for liquid crystal formation in colloidal systems. Indeed it is now known that the presence of anisotropic excluded volume interactions is the main driving force for the formation of mesophases in thermotropic, lyotropic and colloidal systems. In contrast to theory, the first successful simulations of liquid crystals occurred much later. Studies of the simplest phenomenological models did not occur until the 1970s [15], and the first simulations of some of the most common liquid crystal phases, such as the smectic-C, were carried out in the late 1990s [16]; and it is only in the last few years that real progress has been made towards

accurate atomistic simulations and the use of simulation methods to obtain material properties.

In this review article, I highlight some of the recent progress made in the simulation of liquid crystals, concentrating on improvements in atomistic modelling, in the calculation of material properties in bulk liquid crystalline phases, in the modelling of macromolecular materials and in progress made towards bridging across different time and length scales. The paper starts with a brief review of the different models, which are typically employed in the simulation of LC systems.

2. Simulation of liquid crystals: crossing the time and length scales

Arguably, the most difficult problem for molecular simulation today involves linking together simulations which span different time and length scales. As illustrated in figure 1, important phenomena occur at a range of time scales, from the fast bond vibrations in a molecule (which atomistically can be followed with a 1 fs time-step), to rearrangement of the liquid crystalline director in a nematic (which occurs over several ns), to the growth of smectic layers or the rearrangement of small domains

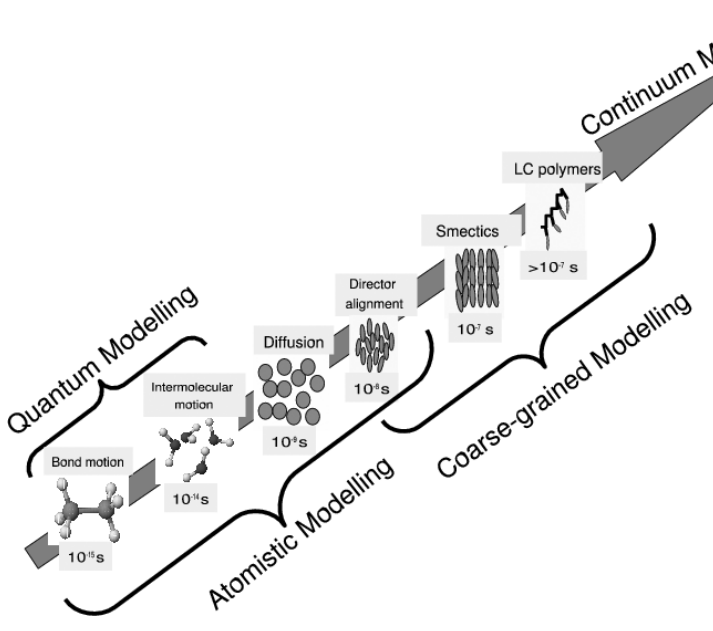

Figure 1. An illustration of the different time scales used in simulation. Molecular bond vibration and intermolecular motion can reasonably be followed with time frames of 1 and 10 fs respectively; diffusion within a molecular liquid usually requires simulations of at least 1 ns; the growth of orientational order and uniform alignment of a nematic director for a few hundred molecules may require up to 10 ns (and this time can be extended considerably for larger system sizes or if the simulation is close to a phase transition); smectics and liquid crystalline polymers will require at least an order of magnitude longer time scales even for small system sizes. There is a whole range of interesting liquid crystalline static and dynamics phenomena, which occur on far longer length scales and time scales than can be studied by molecular simulation. These are best handled by continuum modelling.

in a liquid crystalline polymer (which may take tens or hundreds of ns). This problem is compounded by the length scales required to view different phenomena. Within a molecular description, a few hundred molecules in an approximate volume of $(60\,\text{Å})^3$ may be sufficient to study a nematic phase and to calculate many of the thermodynamic and material properties of that phase. However, several thousand molecules may be required to see convincing smectic layers, or to study the interactions between a liquid crystal and a surface. Further along the length scales, a molecular description starts to become problematic when considering the lengths used in a LC display. A typical layer spacing for a twisted nematic display may be 5 μm or more and a $(5\,\mu\text{m})^3$ slab of nematic would have around 2.4×10^{11} molecules. Here, the number of molecules required is far too large for a molecular level description of a liquid crystal. There are now several excellent approaches for modelling beyond the molecular scale. These include lattice Boltzmann nematodynamics techniques [17–22], minimization of the Landau–de Gennes free energy [23] and continuum theory approaches [24, 25]. Recent work in mesoscopic simulations of liquid crystals has been reviewed by Care and Cleaver [26]. This article will, however, concentrate on molecular level modelling and the next section reviews some of the models currently available.

3. Simulation models for liquid crystal phases

For liquid crystals, the problems posed by different time and length scales has led to a range of computer models being developed. One of the earliest of these was the simple cubic lattice model of Lebwohl and Lasher [15]. Here, a molecular description is eschewed in favour of a nearest neighbour interaction term for a lattice spin which represents the direction of order within a small fragment of nematic liquid crystal. Nearest neighbour sites i and j interact through a potential of the form

$$U_{ij} = -\epsilon P_2\big(\cos\theta_{ij}\big), \tag{1}$$

which is minimized when the angle θ_{ij} between lattice spins is 0° or 180°. As a function of temperature, this model gives rise to a weakly first-order phase transition and a discontinuous change in the order parameter, $S_2 = \langle P_2(\cos\theta)\rangle$. Whereas in 1972 Lebwohl and Lasher were able to study a maximum of 8000 spins ($20 \times 20 \times 20$), today simulations can comfortably look at models with $> 54\,000$ spins, which is sufficient to study structural transitions in nematic thin films [27]. This figure could be pushed relatively easily to several million spins on parallel machines.

Suitable molecular potentials are required to move beyond a lattice description of a liquid crystal phase. Two classes of model have been developed, which have proved particularly popular amongst simulators: hard-nonspherical models and soft-nonspherical models. In the former, hard ellipsoids [28–33] and hard spherocylinders [34, 35] (see figure 2) have been simulated extensively. Hard ellipsoids exhibit nematic ordering and hard spherocylinders exhibit nematic, smectic-A and smectic-B phases. A recent study of three rigidly linked hard spherocylinders has demonstrated the formation of a smectic-C phase [36].

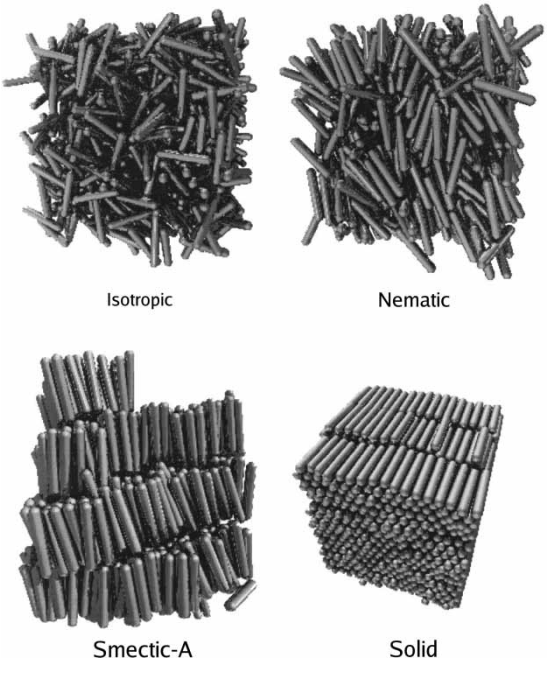

Figure 2. Snapshots taken from simulations of hard spherocylinders with aspect ratio $L/D = 5$ at different densities. Isotropic liquid, nematic, smectic-A and solid phases are shown. Reproduced from figure 2 of reference [35] with permission of the American Institute of Physics.

For hard particle models, temperature is not important and phase behaviour is governed solely by changes in the density. Here the driving force for mesophase formation is the competition between rotational and translational entropy. As density is increased excluded volume becomes more important and the system is able to lower its free energy by aligning and thus increasing translational entropy at the expense of rotational entropy. While this approach may not be fully representative of transitions in thermotropic mesogens, the model certainly captures the essential physics for many colloidal systems. Several reviews of key hard particle simulations have appeared [37, 38].

The most popular soft-nonspherical model is the Gay–Berne (GB) potential [39–45]. Here, the pair-interaction energy is governed by both an anisotropic shape (usually ellipsoidal for the Gay–Berne model) and an anisotropic attraction energy. These features are embodied in a Lennard-Jones (LJ) like potential

$$U_{ij}(\hat{\mathbf{u}}_i, \hat{\mathbf{u}}_j, \mathbf{r}_{ij}) = 4\epsilon_{ij}(\hat{\mathbf{u}}_i, \hat{\mathbf{u}}_j, \mathbf{r}_{ij})\left[\left(\frac{\sigma_s}{r - \sigma(\hat{\mathbf{u}}_i, \hat{\mathbf{u}}_j, \hat{\mathbf{r}}_{ij}) + \sigma_s}\right)^{12} - \left(\frac{\sigma_s}{r - \sigma(\hat{\mathbf{u}}_i, \hat{\mathbf{u}}_j, \hat{\mathbf{r}}_{ij}) + \sigma_s}\right)^{6}\right] \quad (2)$$

where, for particles i and j, the LJ σ parameter and the well-depth parameter ϵ are dependent on both the separation vector, $\mathbf{r}_{ij}$, and the relative orientation of the long axes of the two GB particles, $\hat{\mathbf{u}}_i$, $\hat{\mathbf{u}}_j$. The Gay–Berne potential is characterized normally by four parameters, which determine the overall form of the potential, χ, χ', μ and ν. χ is related to the length σ_e and the breadth σ_s of the molecule; and enters the expression for $\sigma(\hat{\mathbf{u}}_i, \hat{\mathbf{u}}_j, \hat{\mathbf{r}}_{ij})$ and $\epsilon_{ij}(\hat{\mathbf{u}}_i, \hat{\mathbf{u}}_j, \mathbf{r}_{ij})$. μ and ν adjust the shape of the potential and enter the expression for $\epsilon_{ij}(\hat{\mathbf{u}}_i, \hat{\mathbf{u}}_j, \mathbf{r}_{ij})$; and χ' is given by

$$\chi' = \frac{\epsilon_s^{1/\mu} - \epsilon_e^{1/\mu}}{\epsilon_s^{1/\mu} + \epsilon_e^{1/\mu}}, \tag{3}$$

where ϵ_s and ϵ_e are respectively the maximum well depth for the interaction of two GB particles in the side-to-side and end-to-end configurations. Thus GB potentials can be represented by the notation GB(χ, χ', μ, ν), or alternatively, by the notation GB($\kappa, \kappa', \mu, \nu$), where $\kappa = \sigma_e/\sigma_s$ and $\kappa' = \epsilon_s/\epsilon_e$. Examples are shown in figure 3, where U_{ij} is plotted for four different relative orientations of particles using three forms of the potential. As pointed out by Zannoni [44] and others, a choice of GB($\kappa, \kappa', 0, 0$) corresponds to a soft ellipsoid and GB($0, 0, \mu, \nu$) corresponds to a spherical Lennard-Jones potential.

An advantage of the GB model is that it can, in principle, be tuned to represent the interaction of a wide-range of different thermotropic mesogens by adjusting the μ and ν parameters and by changing the relative well depths in figure 3. Gay–Berne models have been developed for disc-like molecules [48] and a variant has been produced for biaxial molecules [49]. Because the GB potential is based on a single site, it is sufficiently cheap to simulate an entire phase diagram [41, 47, 50]. An example is shown in figure 4, which shows the introduction of a smectic-A phase as the potential is lengthened from $\kappa = 3.0$ to $\kappa = 4.0$. In comparison to real thermotropics, there are some disadvantages of this model. Probably the most serious is the fact that following an isobar on figure 4 would lead to a large density change as temperature was increased through the phase transitions Sm $\rightarrow$ N $\rightarrow$ I. In reality however the density changes in real liquid crystals tend to be quite small, around the order of 1% at the nematic–isotropic phase transition. It may be possible to overcome this problem with more realistic parameterizations for the GB potential [51], where the ratios of side-by-side to end-to-end well depths are increased considerably. However, as yet there has been little work on producing full phase diagrams for such parameterizations.

The Gay–Berne model is relatively easy to combine with other potentials and in recent years there have been several interesting studies, including GB + point dipole [52] leading to ferroelectric phases, and GB + point quadrupole leading to a smectic-C phase [16]. These studies are reviewed by Zannoni [44] and by Bates and Luckhurst [53].

One of the powerful features of single site potentials arises from their comparatively low computational cost. This makes it possible to model very large numbers of individual molecules and is particularly useful for studying interfacial phenomena. Consequently, there has been considerable work on studying the properties of liquid crystals in contact with solid surfaces [54–57] and looking at a nematic–isotropic

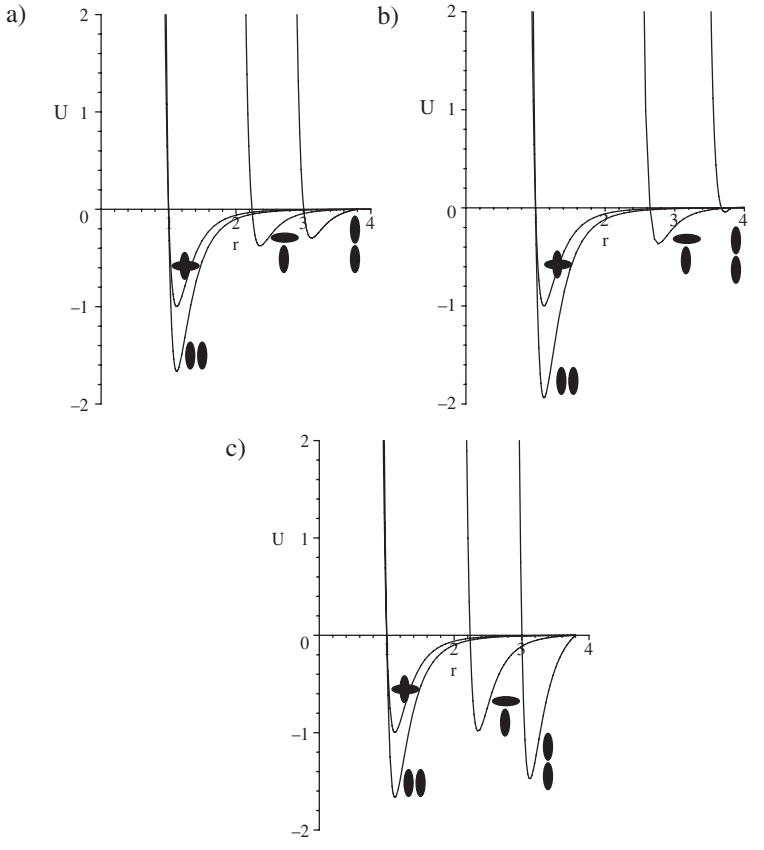

Figure 3. The Gay–Berne potential plotted as a function of four fixed orientations, side-to-side, cross, T-shape and end-to-end, from three variants of the model with $\mu = 2$, $\nu = 1$. (a) $\kappa = 3$, $\kappa' = 5$, (b) $\kappa = 3.6$, $\kappa' = 5$, (c) $\kappa = 3$, $\kappa' = 1$. Graphs are reproduced from data used in figure 1 of reference [46]. The distance r is plotted in terms of σ_s and the potential is plotted in terms of a Lennard-Jones well depth ϵ_o. The form plotted is a cut-and-shifted potential, which is cut at a spherical cutoff of $4\sigma_s$ and shifted to zero at the cutoff. This slightly perturbs the relative well depths of the four potential wells shown at larger distances.

interface [58–61]. The former is of particular practical importance because surface-induced planar or homotropic ordering is used in most liquid crystal displays. Moreover, surface pre-tilt can be used to improve switching in certain display modes and the use of three-dimensional surface features to influence director orientation is being actively investigated as a way of introducing new fast-switching display modes for a new generation of displays.

While this review is principally concerned with thermotropic liquid crystals, it is appropriate here to mention the usefulness of single particle anisotropic potentials in modelling the properties of lyotropic and colloidal systems. Here, concentration changes are extremely important in determining phase behaviour. For example, rod-shaped colloidal particles will form nematic phases characterized by a significant change in the number density of rods at the orientational phase transition. Such transitions are well modelled by single site anisotropic potentials [35].

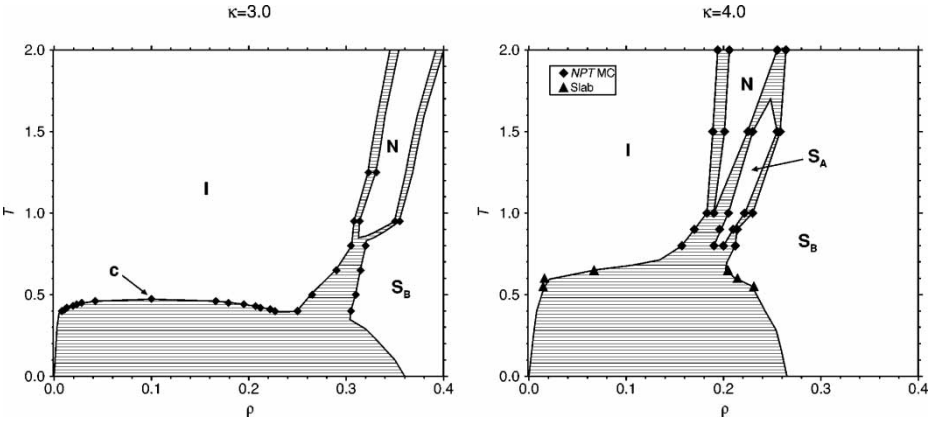

Figure 4. The Gay–Berne phase diagram [47] as a function of molecular elongation for GB($\kappa = 3,\ \kappa' = 5,\ \mu = 2,\ \mu = 1$) (left-hand diagram) and GB($\kappa = 4,\ \kappa' = 5,\ \mu = 2,\ \mu = 1$) (right-hand diagram). The phase diagrams are reprinted with permission from figures 1 and 20 of reference [47]. Copyright 1998 American Physical Society.

At the most realistic end of the modelling spectrum are atomistic models where each atom is represented within a simulation, as shown in figure 5. Here, the full complexity of intra- and intermolecular interactions can be modelled. While a clear disadvantage of this approach is computational cost, this provides the only practical route for studying the influence that subtle changes in molecular structure have on phase behaviour. The early work in this area has been reviewed previously [62, 63]. Below we concentrate on recent progress.

4. Progress in atomistic simulations

The rapid rise in CPU speed over the last 10 years, has vastly improved the capacity to carry out atomistic work, leading to a number of simulation studies of nematics. A decade ago, state-of-the-art work used united atom descriptions, with rather approximate force fields, truncated electrostatic interactions and run lengths of less than 1 ns. Today the state-of-the-art uses *ab initio* derived all-atom force fields, Ewald summation for long-range electrostatics and typical run lengths of at least a few ns or, possibly, several 10 s of ns.

4.1. *Force fields for atomistic simulation of liquid crystals*

Improved force fields for modelling have dramatically improved predictions for all forms of atomistic modelling. Cheung *et al.* [65] have produced a useful LCFF (liquid crystal force field) suitable for many standard calamitic molecules, based on the methodology used by Jorgenson in his work on the OPLS-AA force field for biological systems. The approach is quite simple and easy to extend to other systems. It employs a harmonic force field of the AMBER-type, which is sufficiently flexible

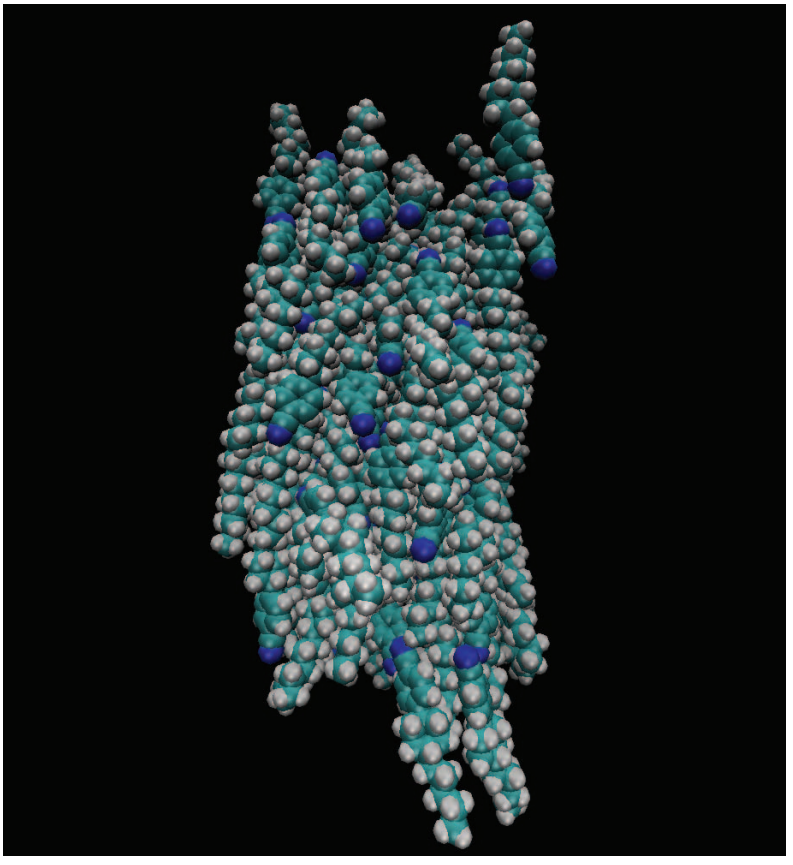

Figure 5. A snapshot taken from a molecular dynamics simulation of the molecule 4-(*trans*-4-n-pentyl-cyclohexyl)benzonitrile (PCH5) in a nematic phase. The molecule is represented at a fully atomistic level and the simulations were carried out by Dr. D. L. G. Cheung [64] at the University of Durham.

to model many calamitic liquid crystals based on relatively simple organic building blocks,

$$E_{\text{ff}} = E_{\text{stretch}} + E_{\text{bends}} + E_{\text{tor}} + E_{\text{vdw}} + E_{\text{elec}}, \tag{4}$$

where the terms in equation (4) have the following forms:

$$E_{\text{stretch}} = \sum_{\text{bonds}} \frac{1}{2} k_l (l - l_{eq})^2, \tag{5}$$

$$E_{\text{bends}} = \sum_{\text{angles}} \frac{1}{2} k_\theta (\theta - \theta_{eq})^2, \tag{6}$$

$$E_{\text{tor}} = \sum_{\text{dih}} \sum_{i} \frac{1}{2} k_i (1 + \cos(i\tau + \delta_i)), \tag{7}$$

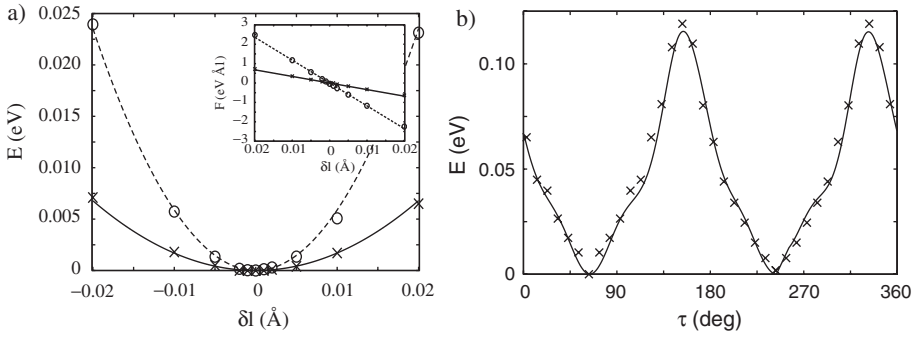

Figure 6. (a) Bond stretching potentials (from [65]) for the C–H bond in biphenyl [the *ab initio* data (×) and the fitted data (-)] and the C–N bond in 4-cyanobiphenyl [the *ab initio* data (◯) and the fitted data (-)]. Inset shows the variation of force with change in bond length, δl. (b) The torsional angle potential (from [65]) for phenylcyclohexane [the *ab initio* potential (×) and the fitted potential (-)]. Reproduced with permission from figures 1 and 5 of reference [65]. Copyright 2002 American Physical Society.

$$E_{\text{vdw}} = \sum_{i,j} 4\epsilon_{ij}\left[\left(\frac{\sigma_{ij}}{r_{ij}}\right)^{12} - \left(\frac{\sigma_{ij}}{r_{ij}}\right)^{6}\right], \tag{8}$$

$$E_{\text{elec}} = \sum_{i,j} \frac{1}{4\pi\epsilon_0}\frac{q_i q_j}{r_{ij}}. \tag{9}$$

Here, intramolecular potentials are used for bond stretching, bond angle bending and torsional interactions; electrostatics are modelled by partial charges interacting through a Coulomb potential (equation 9) and van der Waal's interactions are modelled by a Lennard-Jones 12-6 potential (equation 8). In equations (5)–(9) the symbols take their usual meaning [65], 1-2 and 1-3 non-bonded terms are excluded, and 1-4 interactions are scaled in the usual way.

With today's computer power, good quality *ab initio* calculations can be readily employed to obtain bond stretching, bond bending and torsional potentials. Of these, the latter are crucial, as changes in torsional potential will change molecular shape significantly. So careful fitting must take into account all other terms in the force field during the fitting process [65]. Figure 6 shows bond stretching potentials calculated using density functional theory, with the PW91 GGA functional and a complete plane wave basis set, fitted to obtain force field terms for equation (4). Partial charges can also be obtained from quantum mechanical calculations. Currently, one of the useful approaches to obtaining partial charges comes from fitting to the molecular electrostatic potential obtained via a high-level quantum calculation [66–68].

The 12-6 potential in equation (8) is, of course, approximate and the form of the repulsive term in particular is inaccurate for close approach. However, atoms in fluids sample only the attractive part of the potential and the first part of the repulsive region. Consequently, the 12-6 form works well enough in practise and avoids the need for a more expensive exponential form. Despite recent improvements in calculation of dispersion within *ab initio* quantum calculations, no calculations on liquid crystal fragments are

Table 1. Computed densities and order parameters from a simulation of 216 molecules of 4-(*trans*-4-n-pentylcyclohexyl)benzonitrile (PCH5). Data taken from reference [78].

T/K	$\langle\rho\rangle$/kg m^{-3}	ρ_{expt}/kg m^{-3}	$\bar{S}_2^{\text{inertia}}$	$\bar{S}_2^{\text{expt}}$
300	997.5 ± 7.4	963.0	0.68 ± 0.02	0.63
310	992.9 ± 8.0	956.5	0.65 ± 0.01	0.58
320	981.1 ± 8.1	949.6	0.55 ± 0.03	0.50
330	972.9 ± 10.0	–	0.51 ± 0.04	0.00

likely to capture more than 75% of the dispersion interaction energy. Moreover, even if accurate two-body terms were obtained, the lack of three-body (and higher) forces would prove problematic. Therefore, the best practical approach is to use effective two-body potentials that are fitted to the thermodynamics properties of small molecular fragments; and which therefore take into account many-body effects in an average way. Jorgensen pioneered this approach in his OPLS [69] and OPLS-AA [70] force fields for biomolecules, by fitting the densities and heats of vaporization of small molecules based on a series of bulk phase calculations for molecular liquids. For liquid crystals the approach is equally effective, and potentials fitted in this way transfer nicely to liquid crystal simulations [65]. For the molecule n-4-(*trans*-4-n-pentylcyclohexyl) benzonitrile (PCH5), a comparison of simulated and experimental densities is shown in table 1 using potentials derived via this mechanism. The results are encouraging. Both the densities and average order parameters, $\bar{S}_2 = \langle P_2 \cos\theta \rangle$ (obtained from the long molecular axes defined by the inertia tensor) are good. However, getting the bulk density correct is one of the milestones towards eventually predicting transition temperatures and it seems important that densities are predicted with rather better than 1% accuracy before obtaining accurate transition temperatures becomes a reasonable proposition. Although system size effects may well be significant for a system as small as 216 molecules, it is likely also that a slight over-prediction of the density of the nematic phase leads to the simulated fluid in table 1 remaining nematic at 330 K.

Progress towards polarizable force fields is now being made for some biomolecular force fields, through the use of induced point dipoles [71], fluctuating charges [72, 73] and recently through the use of the classical Drude oscillator model [74, 75]. A move towards the use of these in liquid crystal simulations would also be interesting but such studies have not yet appeared. Likewise, for crystal structure modelling, some progress has been made in using distributed multipoles to improve the description of electrostatic interactions [76]. This would be extremely computationally intensive within an atomistic model of a liquid crystal fluid, if each individual atom was assigned a multipole. Recently, Berardi and co-workers have provided a new algorithm for deriving a set of effective charges to improve the modelling of electrostatic interactions in liquid crystals using only a limited number of interaction sites thereby greatly reducing the computational cost required to include electrostatic terms [77].

4.2. *Prediction of transition temperatures and structure in nematic fluids*

The problems with system sizes and accurate force fields, mentioned above, has not stopped the progress towards the first predictions of transition temperatures. To this

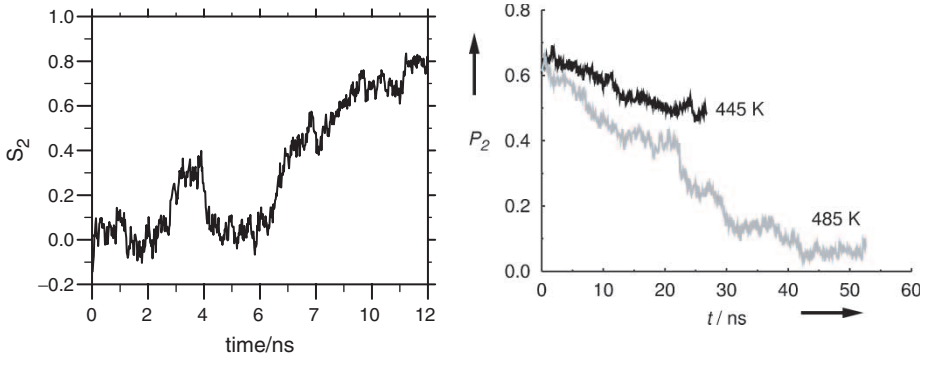

Figure 7. Left: spontaneous growth of nematic order for the molecule 4,4′-di-n-pentyl-bibicyclo[2.2.2] octane (5,5-BBCO) for a state-point in the nematic phase at 300 K (taken from figure 2 of reference [79] reproduced with permission from Taylor & Francis Ltd. http://www.tandf.co.uk). Right: the order parameter ($P_2 = S_2$) for two temperatures for the $n = 2$ homologue of the phenyl alkyl-4-(4′-cyanobenzylidene)aminocinnamate series. (Taken from figure 4 of reference [81] reproduced with permission from Wiley-VCH.)

end, there are two important recent studies. Reference [79] was the first to show the spontaneous growth of a liquid crystal phase from an isotropic phase using atomistic potentials. This is shown in figure 7 for the molecule 4,4′-di-n-pentyl-bibicyclo[2.2.2] octane (5,5-BBCO), where, with a united atom model, an isotropic system is quenched to a temperature well inside the expected range of stability for a liquid crystal phase. Here, spontaneous growth in orientational order occurs over 12 ns. In this study [80], several independent quenches were undertaken each requiring similar run times.

From earlier work on simplified potentials, such as the Gay–Berne mesogen (section 2), one can estimate that 5 ns may be a reasonable time scale for the formation of a nematic from an initial isotropic configuration (growth of order usually occurs in $< 500\,000$ time-steps for GB systems and the reduced time-step in such simulations corresponds to around 10 fs or less of real time). However, the packing in Gay–Berne systems is rather less dense than in real molecules and there are no conformational changes. So time scales for LC growth may be expected to be longer in more realistic models. Unfortunately, close to the phase transition the situation is far worse than one would predict. For the first three members, $n = 0$–3 of the homologous series of alkyl-4-(4′-cyanobenzylidene)aminocinnamates, Zannoni has studied the order of the system, close to the phase transition temperature using an all-atom model. As shown on the right-hand-side of figure 7 for the $n = 2$ system, the simulation times required to check mesophase stability can approach 50 ns.

The structures of the first three phenyl alkyl-4-(4′-cyanobenzylidene)aminocinnamate are shown in figure 8. In these all-atom models, long times are required to sample different conformational states (considerably longer than in the united atom model of 5,5-BBCO mentioned above) and this slows down equilibration. Moreover, if the density for these systems is calculated as a function of temperature (figure 8), it becomes

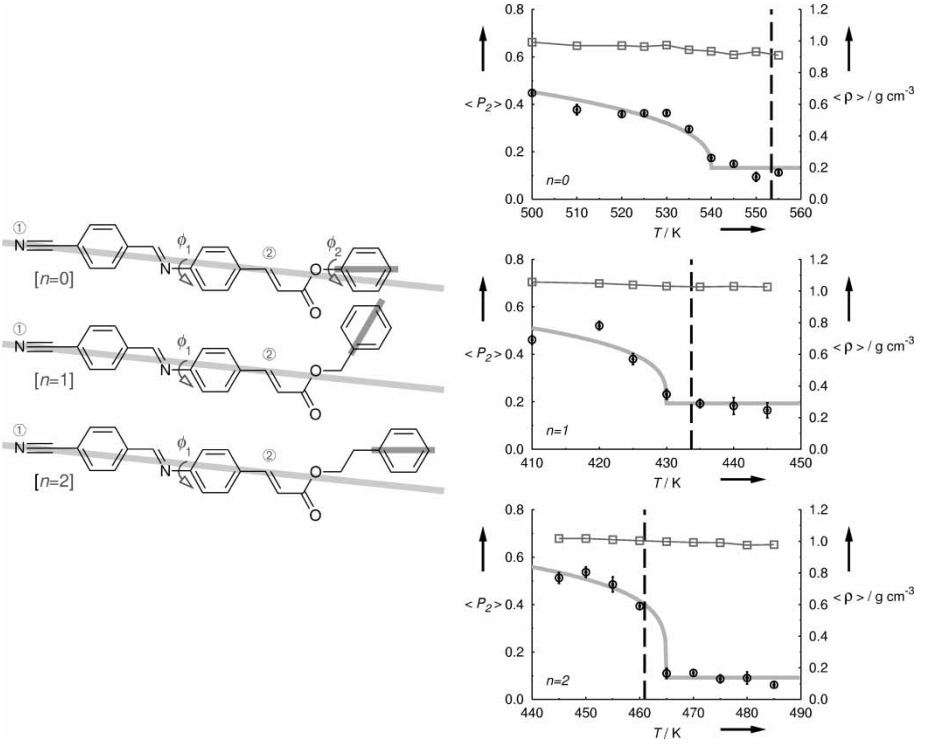

Figure 8. Left: the structures of the first three homologues $n=0$, $n=1$ and $n=2$ of the phenyl alkyl-4-(4′-cyanobenzylidene)aminocinnamate series showing the main rigid molecular axis in the molecule between nitrogen (1) and carbon (2), (taken from figure 1 of reference [81]). Right: the average order parameter (circles) and the average density (squares) as a function of temperature for three phenyl alkyl-4-(4′-cyanobenzylidene)aminocinnamates. The grey line represents a Haller fit to the order parameter $\langle P_2\rangle_{\text{Haller}} = (1-\langle P_2\rangle_{\text{iso}})(1-T/T_{\text{NI}})^{\beta} + \langle P_2\rangle_{\text{iso}}$ for $T \le T_{\text{NI}}$ and assumes a weakly first-order transition for the system. (Taken from figure 6 of reference [81] reproduced with permission from Wiley-VCH.)

clear that this is almost continuous right through the phase transition. While this is gratifying from the point of view of reproducing the behaviour of the real system, the removal of a discontinuous volume change eliminates much of the entropic driving force for mesophase formation seen in the Gay–Berne and hard-particle systems discussed in section 3. (Hence, the need for long time scales in this work.) None the less, the temperature dependent results for the order parameter in figure 8 are very impressive. It now seems possible that clearing temperatures can be predicted to within 15 K or better. For the systems shown in figure 8, Beradi and co-workers are also able to show a convincing odd–even effect, which is often seen in the transition temperatures of many thermotropic LCs. This arises because the structure of the $n=1$ homologue leads to the terminal phenyl ring being unable to adopt a good alignment with the liquid crystal director, something which does not apply for the $n=0$ and $n=2$ homologues.

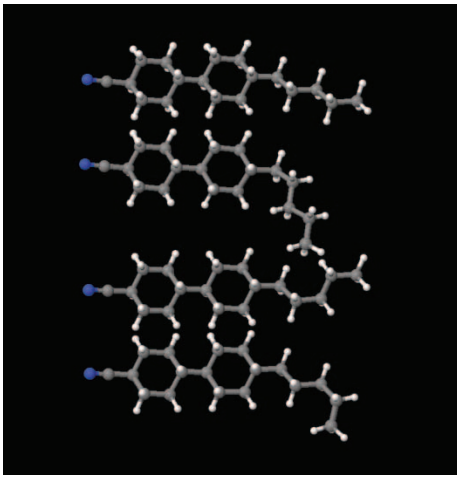

Figure 9. Structure of the molecule CCH5 showing different chain conformations: *ttt*, *gtt*, *tgt*, *ttg*. The introduction of a *gauche* conformation in the even dihedral angle, *tgt*, keeps a linear shape, whereas the introduction of a *gauche* conformation in either of the odd dihedral angles *gtt* or *ttg* leads to a bent molecular shape.

Atom-level simulations allow for the study of changes in molecular structure within a liquid crystal. An early example of this was provided by the work of Wilson and Allen [82, 83], who studied the structure of the molecule *trans*-4-(*trans*-4-n-pentylcyclohexyl) cyclohexylcarbonitrile (CCH5) in the nematic and liquid phases. Here, it is possible to calculate dihedral angle distribution functions, $S(\phi)$, for dihedrals in the C_5 chain as a function of temperature in the two phases. The effects of temperature in changing the Bolzmann distribution for these dihedrals can be addressed by evaluating the underlying effective torsional potential $v(\phi)$, where

$$S(\phi) = \frac{1}{q}\exp\left(\frac{-v(\phi)}{k_B T}\right) \tag{10}$$

for a partition function, q, which is fixed by the minimum of the potential. $v(\phi)$ in the nematic phase shows clearly that *gauche* conformations of odd-dihedrals are less favoured than those of the even dihedral because the former lead to bent structures in which the molecular long axis is unable to align well with the director of the system (figure 9). There is therefore a strong coupling between the internal molecular structure and the structure of the surrounding fluid, which gives rise to an average molecular shape change as the molecule moves between phases. Such an effect is predicted by molecular field theory and helps explain the change in order parameter of C–D bonds within a deuterated chain of a liquid crystal, as studied by NMR [84]. This has been seen now in a number of simulation studies, e.g. [78, 85, 86]. The lack

of this structural change for single site potentials is one of the clear deficiencies in such models.

5. Calculation of materials properties for atomistic and mesoscale models

The importance of optimizing LC material properties is well known. It goes back to the pioneering work of researchers in the 1970s, who realized that the use of LCs in (twisted nematic) displays depended on designing new stable LC molecules with a large dielectric anisotropy. It continued as LCs were optimized further to have the right temperature range, order parameters, elastic constants and viscosity by the painstaking development of suitable mixtures. Initially, this was carried out by trial and error, though a number of empirical rules now exist to guide mixture formulation. Today, the experimental task of developing new LC materials with desired properties remains a huge one, which is made more important by the large range of new applications for LCs, which are currently being explored (see section 1).

From the simulation point of view, prediction of material properties is still in its infancy. However, the last few years have seen some important advances and it seems clear that researchers are much closer to the goal of 'molecular engineering', where simulation can be used to relate molecular structure to bulk material properties and new materials can be designed purely on a knowledge of how changes in molecular structure influence phase behaviour. In this section, some of the recent progress made in the areas of elastic constants, rotational viscosity and helical twisting powers is discussed. The work below concentrates on the practical aspects of obtaining material properties from molecular simulation. The interested reader may also refer to the excellent article by Allen and Masters [87], which reviews some of the underlying theory linking macroscopic variables to microscopic orientational stresses and strains.

5.1. *Elastic constants*

Neglecting surface terms, the distortion free energy of a nematic liquid crystal can be written as

$$F = \frac{1}{2}\int d\mathbf{r}\left[K_1[\nabla \cdot \mathbf{n}(\mathbf{r})]^2 + K_2[\mathbf{n}(\mathbf{r}) \cdot (\nabla \times \mathbf{n}(\mathbf{r}))]^2 + K_3[\mathbf{n}(\mathbf{r}) \times (\nabla \times \mathbf{n}(\mathbf{r}))]^2\right] \qquad (11)$$

where $\mathbf{n}$ is the director and the scalars K_1, K_2 and K_3 are elastic constants [88]. Each elastic constant is associated with a separate mode of distortion of the nematic director: splay – K_1, twist – K_2 and bend – K_3. Any distortion of a nematic therefore carries an energy cost, which depends on the magnitude of the elastic constant(s) associated with it. The length scales normally associated with director distortions are long compared to the molecular scale. Despite this, the elastic constants have an underlying dependence on the molecular interactions of nematogens themselves. It is therefore possible to change elastic constants by changing molecular interactions. In all liquid

crystal displays the electro-optic switching depends on a field-induced distortion of the director; and, in most current commercial displays, the relaxation of director back to an undistorted state relies wholly on elastic restoring forces (i.e. is not switched). Consequently, elastic constants are one of the key bulk properties that determine the behaviour of LC materials in electro-optical devices.

There are a number of techniques that can be used to obtain K_1, K_2 and K_3. In common with other material properties, it is possible to mimic the setup for experimental measurements within a simulation. For elastic constants this involves studying a Freedericsz-like transition within a simulation by perturbing a slab of simulated liquid crystal with an orienting field; or, more subtly, by perturbing the system with an orienting field which varies sinusoidally in space with a specified wavenumber [89]. Alternatively, it is possible to sit at equilibrium in a simulation and to monitor the wavelength dependence of thermally excited orientational fluctuations. An early paper by Cleaver and Allen [89] compared such methods for the simple Lebwohl–Lasher lattice model (section 3), studying a system of over 32 000 particles. They conclude that the different methods provide consistent results. However, the orientational fluctuation method gives rather better statistics and is suitable for study with relatively small numbers of molecules. It is therefore far more applicable for study with off-lattice models.

In the orientational fluctuation method, elastic constants can be obtained by first calculating the ordering tensor in reciprocal space

$$\hat{Q}_{\alpha\beta}(\mathbf{k}) = \frac{V}{N}\sum_{i=1}^{N_m}\frac{3}{2}\left(u_{i\alpha}u_{i\beta} - \frac{1}{3}\delta_{\alpha\beta}\right)\exp(\mathrm{i}\mathbf{k}\cdot\mathbf{r}_i), \tag{12}$$

where $\mathbf{k}$ is a wavevector of the simulation box and the sum is taken over all molecules, N_m. $\mathbf{Q}(\mathbf{k})$ is then transformed into the director-based frame with $\mathbf{n} = (0, 0, 1)$. In this coordinate system, the orientational fluctuations can be written as

$$\left\langle \hat{Q}_{13}(\mathbf{k})\hat{Q}_{13}(-\mathbf{k})\right\rangle = \left\langle \left|\hat{Q}_{13}(\mathbf{k})\right|\right\rangle = \frac{(9/4)\langle S_2\rangle V k_B T}{K_1 k_1^2 + K_3 k_3^2}, \tag{13}$$

$$\left\langle \hat{Q}_{23}(\mathbf{k})\hat{Q}_{23}(-\mathbf{k})\right\rangle = \left\langle \left|\hat{Q}_{23}(\mathbf{k})\right|\right\rangle = \frac{(9/4)\langle S_2\rangle V k_B T}{K_2 k_1^2 + K_3 k_3^2}, \tag{14}$$

which are valid in the limit of small k. Plotting

$$W_{13}(k_1, k_3) = \frac{(9/4)\langle S_2\rangle V k_B T}{K_1 k_1^2 + K_3 k_3^2} \tag{15}$$

as a function of k_1^2 and k_3^2 provides a surface from which a fit to a bivariate polynomial in k_1^2 and k_3^2 can be made. K_1 and K_3 can be extracted from the fit. In a similar way, plots of

$$W_{23}(k_1, k_3) = \frac{(9/4)\langle S_2\rangle V k_B T}{K_2 k_1^2 + K_3 k_3^2} \tag{16}$$

Table 2. Elastic constants from Gay–Berne mesogens calculated via the orientational fluctuation method. Data are taken from reference [90] with permission from the American Institute of Physics. Pairs of K_1, K_3 values calculated from W_{13} are given along with pairs of K_2, K_3 values calculated from W_{23}. Estimated statistical errors in the final digit(s) are given in parentheses.

GB model	ρ^*	T^*	K_1	K_3	K_2	K_3	$\langle S_2 \rangle$
GB(3,5,2,1)	0.32	0.90	0.652(33)	2.01(08)	0.676(55)	2.01(10)	0.674(2)
GB(3,5,2,1)	0.33	1.00	0.697(74)	2.59(19)	0.718(42)	2.27(20)	0.708(13)
GB(3,5,2,1)	0.35	2.00	1.511(25)	4.79(15)	1.099(98)	5.23(18)	0.663(3)
GB(3,5,2,1)	0.38	3.00	3.55(14)	13.5(1)	2.53(12)	13.0(5)	0.730(5)
GB(3,5,1,3)	0.30	3.40	2.17(12)	3.97(6)	1.71(11)	3.95(6)	0.553(5)
GB(3,5,1,3)	0.30	3.45	1.59(2)	2.23(8)	1.34(2)	2.19(10)	0.478(5)

yield K_2 and K_3. Results from this method are shown in table 2 for two Gay–Berne models GB($\kappa = 3, \kappa' = 5, \mu = 2, \nu = 1$) and GB($\kappa = 3, \kappa' = 5, \mu = 1, \nu = 3$). All three elastic constants increase with density for similar values of the order parameter. For fixed density, the two state points for the GB($\kappa = 3, \kappa' = 5, \mu = 1, \nu = 3$) system show the expected fall in elastic constants with increasing temperature/decreasing $\langle S_2 \rangle$. An important point to note from table 2 is that in some cases the twist elastic constant, K_2, is larger than K_1. In comparison, most nematogens used in displays have $K_3 \approx K_1 > K_2$ (with $K_3 > K_1$ as temperature is cooled towards a nematic to smectic phase transition). In section 2, it was pointed out that there were unrealistic features in the phase diagram of a GB(3, 5, 2, 1) particle. The relatively low K_1/K_2 ratio is also a feature of the model and this can probably be attributed to the low value of $\kappa' = 5$ compared to what is expected for many real mesogens. This is manifested in a relatively small difference in the side-to-side and T-shape potential wells plotted in figure 3.

While the director fluctuation method provides an excellent robust method for determining the elastic constant with quantifiable errors, there have been other methods developed that can also be applied to off-lattice systems. Most prominent are studies based on the direct correlation function (DCF) of a nematic. While approximate theories exist for the latter, it has recently become possible to calculate the DCF for a nematic from simulation without approximation. In seminal work [91, 92], Schmid and co-workers show how to obtain the DCF for a nematic by taking into account the dependence of pair correlations on the orientation of the director. The DCF can then be used to obtain K_1, K_2 and K_3 from the Poniewierski–Stecki formulae [93]. As a comparison, Schmid and co-workers have calculated elastic constants for a system of soft ellipsoids [91] and compared the results for this technique with the orientation fluctuation method, obtaining good agreement. There have also been techniques developed to obtain K_2 directly from simulation, most notably from the torque density in a simulated chiral nematic [94], from a simulation of the Freedericksz transition [95] and a new technique involving a two-particle average in a homogeneous nematic [96].

The consistency of results from the best studies give a high degree of confidence in the methods. However, the relatively large number of molecules required means that it is difficult to apply the techniques to atomistic studies with any degree of certainty. In particular, for the director fluctuation technique, system sizes of around 16 000 are required to generate a substantial uncurved section in the 3D surface plots of

$W_{13}(k_1, k_3)$ and $W_{23}(k_1, k_3)$. While fits for smaller system sizes of around 2000 may be possible, this remains a large number of molecules for atomistic level simulations. Moreover, statistics are much poorer if the director is unconstrained and free to diffuse in response to thermal excitation (director constraints are not easy to implement at the atomistic level). Similarly, the DCF method requires knowledge of the DCF over large distances (low k). Additionally, $C(1, 2)$ is typically of the range of the intermolecular interaction, which would become very large for atomically detailed systems with long-range electrostatic interactions. However, with recent increases in computer speed, it should now be possible to explore the relationship between molecular potential and elastic constants by coarse-graining from atomistic to mesoscale models; and then using the director fluctuation or the DCF methods to obtain the elastic constants. Such studies have yet to be carried out.

5.2. *Rotational viscosity*

The switching times for a liquid crystal in a electro-optic device depend on the rotational viscosity γ_1. For example, on and off times for a twisted nematic display are directly proportional to γ_1. There are a number of possible routes to γ_1 involving equilibrium and non-equilibrium molecular dynamics. In the former, a normal MD simulation is carried out and an appropriate Green–Kubo integral is worked out while the system remains at equilibrium. In the latter the system is coupled to the field [97]. Much of the early work on rotational viscosities was carried out on simple single site potentials, such as the Gay–Berne potential [97–99].

Non-equilibrium methods are not particularly attractive for atomistic simulations, as the director must be constrained or reorientated and these tasks are not simple at an atomistic level. However, equilibrium methods are more accessible. Using linear response theory, Sarman and Evans [97] showed that γ_1 can be found from the integral of the director angular velocity correlation function by

$$\gamma_1 = \frac{k_B T}{V \int_0^\infty dt \langle \Omega_2(t) \Omega_2(0) \rangle}, \tag{17}$$

where T is the temperature, V is the volume, k_B is Boltzmann's constant, and Ω_2 is obtained from the director angular velocity, $\boldsymbol{\Omega} = \mathbf{n} \times \dot{\mathbf{n}}$, transformed into a frame of reference with the director along the z-axis, such that

$$\boldsymbol{\Omega} \rightarrow (\Omega_1, \Omega_2, 0). \tag{18}$$

Using the molecular long axes, obtained from the inertia tensor, to calculate the director vector, $\mathbf{n}$, equations (17) and (18) can be evaluated by monitoring director fluctuations during an equilibrium simulation.

From the rapid decay of this correlation function shown in figure 10(b), it would seem that this would be extremely promising as a method of extracting γ_1 values, requiring only short simulation times. However, in reality the form of the decay function shown here emerges from noise only after careful time-averaging from run lengths

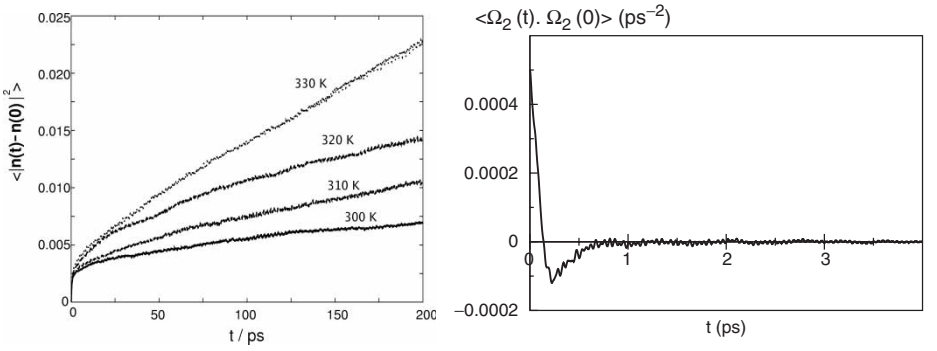

Figure 10. (a) Director mean squared displacements from simulations of 125 PCH5 molecules at four temperatures. (b) Angular velocity correlation function for the liquid crystal director of PCH5 at 310 K [101]. Reprinted from reference [101] with permission from Elsevier.

of several nanoseconds. So there is no way of circumventing the need for extremely long simulations in the pursuit of rotational viscosities.

As an alternative to equations (17) and (18), γ_1 can be obtained from calculations of the director mean squared displacement, $\langle n_2^2(t)\rangle = \langle|\mathbf{n}(t) - \mathbf{n}(0)|^2\rangle$, in the long time limit

$$\frac{\gamma_1}{2} = \lim_{t\to\infty}\lim_{V\to\infty}\frac{k_B T t}{V\langle n_2^2(t)\rangle}, \tag{19}$$

as shown in figure 10(a) for a series of temperatures in an atomistic simulation of PCH5. For most methods, it would be desirable to test the size dependence of these results, especially in the light of the $V \to \infty$ limit in equation (19). While this has been done for GB fluids [100], at an atomistic level it is beyond current computational limits to test the size dependence of the results by employing a series of successively larger simulations. None the less the two methods appear to give comparable results and a direct comparison with experiment for PCH5 (figure 11) points to this being a promising way of obtaining γ_1.

It is possible also to obtain γ_1 from calculations of the rotational diffusion (RD) coefficient, as described by Zakharov and co-workers [103, 104], and by forcing the nematic director to rotate under the influence of an external field [105]. These have been shown to give good agreement with experiment. However, in the case of the RD method, the effect of approximations used in the solution of the appropriate kinetic Fokker–Planck equation are not fully clear. A detailed analysis of all these approaches and their system size dependence would be pertinent.

5.3. *Helical twisting powers*

When chiral molecules are added in an achiral nematic, they transmit their chirality to the whole system. The effect is long range, resulting in a left-handed or right-handed chiral nematic phase with a helical twist, which can be characterized by a pitch, P. Opposite enantiomers are found to induce opposite twists in the nematic host.

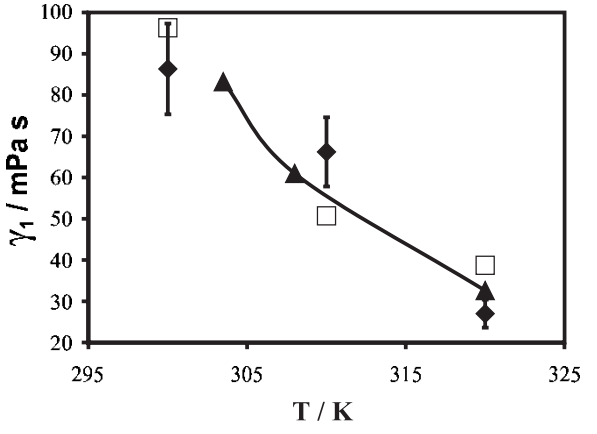

Figure 11. Comparison of calculated and experimental values of γ_1 for PCH5. Theoretical results from reference [101] (squares – from equation 19, diamonds – from equation 17). Experimental results (triangles) taken from reference [102].

The sign of the twist induced is related to the nature of the intermolecular interactions between dopant and solvent, and is shown below to be closely related to molecular shape. The effect is uncorrelated to the optical activity of enantiomers in an isotropic solution. Different molecules are known to induce different levels of twist in a host phase. This can be measured through a property known as the helical twisting power (HTP), β_M, where

$$\beta_M = (Pc_w r)^{-1}. \tag{20}$$

Here, c_w is the weight concentration of chiral dopant and r is the enantiomeric purity of the dopant. Chiral molecules with very high HTPs ($>100\,\mu m^{-1}$) have significant technological applications. They can be used in liquid crystal displays and in chiral polymer films to improve the viewing angle of a display [106–108]. There are also possible applications in polymer-stabilized blue phases [6], which may provide a new generation of devices: fast light modulators and tunable photonic crystals.

Nordio, Ferrarini and co-workers [109–116] have developed a useful theoretical model to link structure with HTP. In their surface chirality model it is assumed that the alignment of a solute molecule in a locally nematic environment can be determined from the shape of the solute molecule. It is therefore the chiral nature of the molecular surface which exerts a torque on the local nematic director. This is transmitted over distances many times its molecular length due to the elastic properties of the nematic phase. In the theory the value of β_M can be found from

$$\beta_M = \frac{RT\varepsilon\chi}{2\pi K_2 v_m} = D\chi, \tag{21}$$

where ε, v_m and K_2 are, respectively, the strength of the orienting potential, the molar volume of the nematic solution and the twist elastic constant of the solvent.

Table 3. Diagonal components of the helicity tensor **Q**, and the ordering matrix **S**, chirality order parameter χ, and experimental helical twisting powers β_M from references [118, 119] for the bridged biaryl molecule (1–8) and helicene molecules (M1–M4). Calculated values are taken from reference [117] with permission from the American Institute of Physics.

Molecule	Q_{xx}	Q_{yy}	Q_{zz}	S_{xx}	S_{yy}	S_{zz}	χ/Å^3	β_M/μm^{-1}
1	−103	79	24	0.05	−0.37	0.31	+21.9	+69
2	90	−67	−23	0.06	−0.38	0.31	−19.2	−65
3	24	−85	62	0.03	−0.33	0.31	−39.1	−71
4	125	−101	25	−0.02	−0.32	0.35	−17.1	−55
5	92	−63	−29	0.12	−0.38	0.26	−22.4	−21
6	−116	92	25	0.02	−0.35	0.33	+21.6	+85
7	−137	93	45	0.06	−0.31	0.26	+21.0	+80
8	−124	67	57	0.14	−0.33	0.19	+23.4	+79
M1	69	−68	−1	0.04	−0.39	0.36	−23.6	−55
M2	61	−44	−17	−0.04	−0.37	0.40	−5.8	−9
M3	37	−55	18	0.05	−0.39	0.34	−23.8	−20
M4	41	−50	9	−0.01	−0.39	0.40	−18.2	−13

The quantity χ is defined as the chirality order parameter and describes the coupling between the chiral surface of the molecule and its orientational ordering. Positive values of χ lead to a right-handed twisted nematic being induced in the liquid crystal host. Calculation of χ requires three tensors: a surface tensor **T** obtained from a Connolly molecular surface, a helicity tensor **Q** representing the twisting power of the surface and an ordering tensor **S** obtained from the orientational distribution function of the molecule. The latter depends on a mean field orienting potential in which the surface normal at each point on the surface lowers its interaction energy if it can lie perpendicular to the local nematic director. In this approach

$$\chi = -\left(\frac{2}{3}\right)^{1/2}\left(Q_{xx}S_{xx} + Q_{yy}S_{yy} + Q_{zz}S_{zz}\right), \tag{22}$$

where the diagonal components of S_{ii} and Q_{ii} are obtained by expressing **S** and **Q** in the principal axis system of the surface tensor **T**. The theory is described in more detail elsewhere [110, 115–117]. Thus the HTP depends, not only on the intrinsic twisting power of the molecule itself, but also on the ordering of the molecule in the nematic host. The success of the theory is shown for a set of rigid chiral dopants in table 3. Here, the sign of χ is correct in all cases and if the value of D is set by reference to an experimental best fit, β_M is predicted with an average error of $\pm 16\,\mu\text{m}^{-1}$ [117].

In addition to the chirality order parameter, there are other methods of studying HTPs. Recent success has been achieved with a scaled chiral index [120, 121] and a mean field approximation that takes into account chiral dispersive interactions [122]. In the case of the former, no account is taken of the surrounding fluid. Instead, HTP is seen as an intrinsic property of a molecule, which is proportional to the index

$$G_{0S} = \frac{4!}{3N^4}\left[\sum_{\text{all permutations of } i,j,k,l=1\cdots N} w_i w_j w_k w_l \times \frac{\left[\left(\mathbf{r}_{ij}\times\mathbf{r}_{kl}\right)\cdot\mathbf{r}_{il}\right]\left(\mathbf{r}_{ij}\cdot\mathbf{r}_{jk}\right)\left(\mathbf{r}_{jk}\cdot\mathbf{r}_{kl}\right)}{\left(r_{ij}r_{jk}r_{kl}\right)^n r_{il}^m}\right], \tag{23}$$

where w_i, w_j, w_k, w_l are atomic weights associated with atoms $i-l$ (normally set to 1.0 for HTP measurements) and the use of $n=2$ and $m=1$ produces a dimensionless index. While the results from this index are normally very good [120, 121], in a few molecules this approach has been seen to go spectacularly wrong. When a molecule contains a rigid chiral core and a flexible achiral chain, the chirality of the core atoms can continue to add a large term to the sum in equation (23) even when atoms are a considerable distance from the core [123]. This can be prevented by introducing a cutoff to the distances employed in equation (23). The use of a cutoff may physically relate to the influence of the chiral molecule on surrounding solvent molecules, even though no solvent/solute interactions appear in the theory. That is, beyond certain separation distances a combination of four atoms cannot reasonably exert a twist on a neighbouring solvent molecule, so the contribution from the four atoms should not be included in the evaluation of equation (23). Kamberaj *et al.* [124] have recently looked at the relationship between χ and G_{0S}, showing that each quantity is sensitive to different aspects of chirality in a molecule. Moreover, they show that a whole series of surface indices are possible and may be necessary to represent all aspects of chirality for any generalized structure. However, the physical relation of each index to experimentally measureable quantities, such as HTP, remains an open question.

An interesting extension to the Nordio–Ferrarini theory comes from examining how χ varies with conformation, through an internal Monte Carlo approach [125]. Not only does this provide a route to calculating β_M for flexible molecules, it also provides some intriguing insights into chirality. χ is seen to vary considerably with molecular conformation and even to change sign. Moreover, because the balance of conformations in a molecule usually changes with temperature, this leads to the prediction of a temperature dependent β_M. In the extreme case, where high temperature conformers have the opposite sign of β_M to those preferred at low temperature, Earl and Wilson have shown [125] that the changing balance of conformations can explain the remarkable property of helical twist inversion which can occur in some chiral nematic materials [126, 127].

Thisayukta *et al.* have reported the experimental observation that doping a chiral solvent with an achiral banana molecule leads to an increase in the twist of the phase [128]. Looking at the achiral bananas with the combined chirality tensor/Monte Carlo technique provides an interesting insight [125, 129]. Individual conformations of bananas, such as the one shown in figure 12, can exhibit extraordinary large values of χ, which arise when the molecules themselves twist into a helical shape. It therefore seems likely that in a chiral solvent, the helical conformations which want to twist with the solvent have a lower free energy and are preferentially selected in favour of their enantiomers, leading to an increase in the twist of the phase. If this is true, this would mean that preferential selection of chiral conformations is being mediated by the chirality of the host phase: a surprising result.

In the majority of experimental measurements of β_M, it is usually found that β_M is solvent independent (see below for reasons). There are, however, a few cases where the sign of β_M has been reported to change with a change in solvent polarity. Here it seems likely that the dramatic change in β_M arises from a change in the balance of conformers induced by specific solute–solvent interactions. The single molecule surface chirality model, of equation (21), only considered the interaction with the solvent through

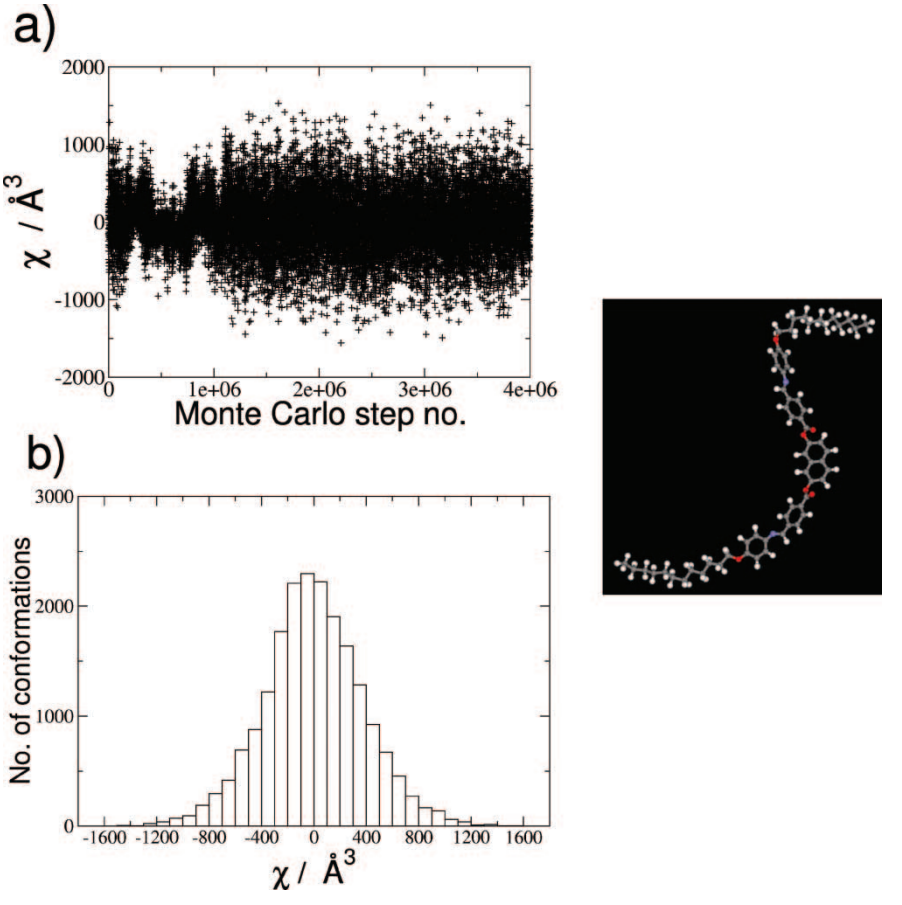

Figure 12. Left: the distribution of χ values from a Monte Carlo simulation of an achiral dopant. Top: variation of χ through the course of a simulation. Bottom: histogram of the distribution of χ values. Right: an individual chiral conformation corresponding to a helical shape [129]. Figure reprinted with permission from figures 4 and 5 of reference [129]. Copyright 1998 American Physical Society.

the presence of a mean field interaction term ϵ. However, it would be desirable to attempt to develop methods to include the influence of solute–solvent interactions. To this end there have been promising theories developed by Allen and co-worker with associated trial simulations for single site potentials [94, 130]. In the first of these theories [130] it can be shown that, if an enantiomer is immersed in a nematic solvent with a uniform twist given by a wavevector k, ($P = 2\pi/k$), there is a chemical potential difference, $\Delta\mu$, between the enantiomer and its mirror image in the same twisted solvent. This arises because the enantiomer which *wants to twist* in the same direction as the phase will have a lower free energy. In the limit of low k, the helical twisting power is directly proportional to $\Delta\mu$ and inversely proportional to the twist elastic constant of the bulk phase

$$\beta = \frac{\Delta\mu}{8\pi K_2 k}, \tag{24}$$

with

$$\beta_M = \frac{2N\beta}{Vc_w}. \tag{25}$$

K_2 can be obtained by the methods described in section 5.1 but in practice many nematic solvents have similar K_2 values. Consequently, a comparison of $\Delta\mu$ values would be sufficient to extract out relative HTP values. Wilson and co-workers have tested both theories for a group of rigid dopants in generic solvents represented by Gay–Berne [131] and soft repulsive spherocylinder models [132]. To calculate $\Delta\mu$ the enantiomers are grown into a twisted solvent in a sequence of Monte Carlo simulations where the chiral solute is gradually introduced into the twisted solvent. Using a highly twisted solvent to increase $\Delta\mu$, the approach is seen to work quite well, predicting the correct sign of $\Delta\mu$. However, the changes in $\Delta\mu$ are less than $1\,\mathrm{kJ\,mol^{-1}}$ from free energy changes that are closer to $20\,\mathrm{kJ\,mol^{-1}}$ for each growth sequence; hence the error bars for calculated HTPs are large. Consequently, the approach would be rather difficult to extend to flexible molecules, where obtaining accurate conformational averaging would make it harder to obtain precise results.

An interesting alternative approach to obtaining HTPs in a solvent was introduced by Germano *et al.* [94]. Here, a method is presented to obtain the equilibrium pitch wavenumber, q, and the twist elastic constant, K_2, of a chiral nematic liquid crystal simultaneously by sampling the torque density. The method requires simulations of a dopant in both a twisted and untwisted solvent. If K_2 is already known, then for a dopant with weight concentration, c_w, in an untwisted nematic of volume, V, the HTP can be obtained from the expression

$$\beta_M = \frac{\langle \Pi_{zz} \rangle_{0,\lambda}}{2\pi c_w V K_2}, \tag{26}$$

where $\langle \Pi_{zz} \rangle_{0,\lambda}$ is the torque density measured with the nematic director constrained to the x, y plane. Earl and Wilson [117] have shown that this expression can be applied to a series of atomistic rigid dopants in a generic Gay–Berne solvent. As K_2 has been calculated already for suitable GB state-points, a single calculation evaluating $\langle \Pi_{zz} \rangle_{0,\lambda}$ in a nematic solvent is sufficient to obtain β_M. This method removes the need for twisted periodic boundary conditions and gives reasonable values for β_M. As with the $\Delta\mu$ method, the real computational challenge is in obtaining really good statistics in the measurement of relatively small quantities. As yet this method has not been applied to solvents which are modelled at an atomistic level but if the statistics were favourable, it may provide an interesting route to the study of chiral interactions.

6. Coarse-grained simulations for complex liquid crystalline materials

6.1. *A coarse-grained model for flexible macromolecular liquid crystals*

There are still severe size limits imposed on atom-level studies, which make it difficult to use such calculations for high molecular weight liquid crystals. None the less, questions

about the molecular organization within a LC phase, the presence or absence of microphase separation and the role played by molecular interactions in influencing material properties are fundamental questions to pose. None of these questions can be answered by a continuum level description of the system, and so the development of suitable coarse-grained models becomes important.

A good practical approach to such systems is provided by the coarse-grained model of Wilson and co-workers [133, 134], which combines anisotropic potentials that are commonly used for mesoscale simulation, with Lennard-Jones sites. In practice this is done by using a force field such as equation (4) with the addition of extra terms for anisotropic sites. Equation (8) is rewritten as

$$E_{\mathrm{vdw}} = \sum_{i=1}^{N_{\mathrm{at}}} \sum_{j>i}^{N_{\mathrm{at}}} U_{ij}(\epsilon_{ij}, \sigma_{ij}) + \sum_{i=1}^{N_{\mathrm{at}}} \sum_{j=1}^{N_{\mathrm{GB}}} U_{ij}(\epsilon_{ij}, \sigma_{ij}) + \sum_{i=1}^{N_{\mathrm{GB}}} \sum_{j>i}^{N_{\mathrm{GB}}} U_{ij}(\epsilon_{ij}, \sigma_{ij}) \tag{27}$$

for N_{at} isotropic sites and N_{GB} anisotropic sites, plus additional harmonic 'GB-angle' interaction terms, of the form shown in equation (6), where the angles θ and θ_{eq} are defined in terms of the angle between a bond to a neighbouring particle and a fixed axis in the anisotropic particle (such as the long axis in a uniaxial particle). Depending on the degree of coarse-graining involved, the bond angle bending and torsional terms can be removed and bond-stretching terms can be replaced by a FENE-type soft potential. Typical choices for anisotropic potentials could be soft-repulsive spherocylinders [135] or Gay–Berne particles, as these are already known to be good for low molecular weight liquid crystals and are differentiable to provide forces and torques or gorques for use in molecular dynamics simulations with leap-frog [136] or Verlet type integration schemes for anisotropic sites [137]. However, if differentiable analytic forms are not needed, (for example in a Monte Carlo simulation), digitized tabulated coarse-grained potentials, which are non-continuous, can be used instead [138].

It is worth noting that electrostatic interactions can also be used in this type of coarse-grained model. In practice, however, one of the common aims of coarse-graining is to remove the electrostatic interactions (which are long-range and therefore expensive to compute) wherever possible, or, in cases where a removal of electrostatics interactions would be unphysical, to simplify from multiple sites containing partial charges to a smaller number of coarse-grained sites containing embedded dipoles.

It should be noted also that coarse-graining methods for thermotropic liquid crystals are not unique and many of the techniques used for liquid crystals can be used for polymers and other complex fluid systems. For example, a coarse-grained model using several Gay–Berne sites has been used by Essex and co-workers in a recent study of the hydrocarbon region of a biomembrane [139]; membrane simulations with coarse-grained isotropic potentials have been reviewed by Saiz and Klein [140]; and recent simulations by Marrink, Mark and co-workers provide impressive demonstrations of self-assembly of model lipids into bilayers and vesicles [141–145]. There has also been considerable simulation work on amphiphilic polymer chains [146, 147] and rod-coil diblock copolymers [148]. Important in the latter work has been the use of dissipative particle dynamics (DPD) techniques [149, 150] to provide a way of

speeding up the equilibration of complex phases. Inherent in the DPD work is the employment of underlying ultra-soft-potentials, allowing particles to pass through each other and thereby improving equilibration times greatly. Such technique have recently been exploited by Levine *et al.* [151] and Gomes and co-workers [152] to study nematic and smectic mesophases.

6.2. *Liquid crystal polymers*

Liquid crystal polymers (LCPs) fall into two main classes [153]. Main chain liquid crystal polymers (MCLCPs) normally incorporate rigid mesogenic groups within the polymer backbone. In contrast, side chain liquid crystal polymers (SCLCPs) contain mesogenic moieties as pendant groups linked to the backbone via flexible spacers [154]. The latter decouples the mesogens slightly from the backbone conformation; however, the backbone still exerts a significant influence on mesomorphism. There is considerable room for chemical modification to control properties. Thus in SCLCPs, the structure of the pendant mesogenic groups, the nature of the polymer backbone, the molecular weight, the tacticity and the length of the flexible spacer length all exert an influence on mesophase formation.

The hybrid anisotropic/isotropic group model, described above, naturally lends itself to polymeric systems. Individual mesogenic groups can be replaced by a Gay–Berne particle and the polymer chains can be modelled by a collection of united atom groups. One of the first main chain simulations studied short polymer chains of the form shown in figure 13. For $m = 6$, $n = 10$, it proved possible to spontaneously see the formation of a nematic phase on cooling from an isotropic melt, as shown in figure 13. As in real main chain polymers, an odd–even dependency of thermodynamics properties on spacer length was seen in the simulation results.

A similar hybrid model provides some interesting insights into the molecular structure within a SCLCP [156]. If the polymer is cooled down from a high-temperature anisotropic melt at 500 K, microphase separation starts to occur, with the mesogenic groups forming domains, which are isolated from each other by the polymer backbone (figure 14a). Further cooling and annealing leads to the mesogenic moieties within these domains aligning; and if the polymer is annealed in the presence of an external ordering potential (mimicking an applied magnetic field) a uniformly aligned liquid crystal is formed (figure 14b,c). In the annealing process, the polymer backbone is excluded from the liquid crystalline layers, becoming confined into regions of about the same dimension as a single smectic layer. In so doing it completely loses its random coil conformation, which is seen in the high temperature isotropic melt, leading to a high anisotropy in the backbone radius of gyration. Such a result ties in closely with the interpretation of experimental X-ray diffraction [157], neutron diffraction [158, 159] and small angle neutron scattering (SANS) [158–166] data.

An interesting result from the simulations is that the flexible spacer, which links the backbone to the mesogenic units, appears to be excluded into sublayers either side of the polymer backbone (figure 14b,c), a phenomenon which would be difficult to 'see' experimentally. Defects in the lamellar structure are seen also in the simulations and the extent to which these occur is influenced strongly by the rate of cooling. In a typical defect (seen in figure 14c) the polymer backbone bridges across a mesogenic region.

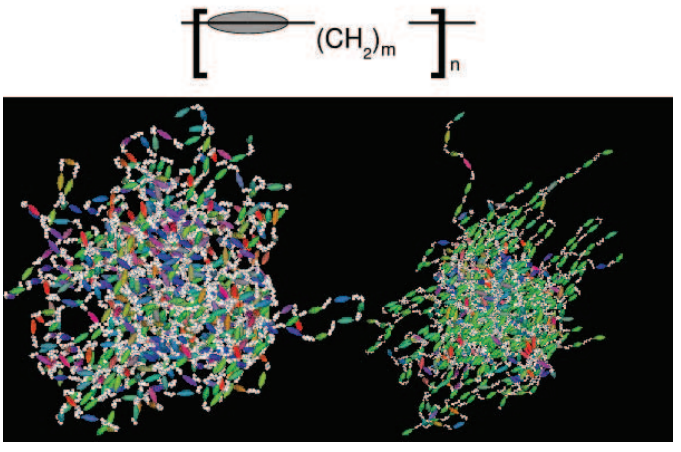

Figure 13. Snapshots showing the structure of a model main chain liquid crystalline polymer for the model system with $m=6$ and $n=10$. Left: isotropic phase at 500 K. Right: the nematic phase at 350 K. Isotropic groups are shown in white. Anisotropic groups are colour coded with green along the director. Pure RGB colours represent mutually perpendicular directions. Figure drawn using simulation results taken from reference [155].

In doing so, the well-ordered smectic layers are disrupted, leading to nematic ordering of mesogenic groups in the neighbourhood of the defect.

6.3. *Liquid crystal dendrimers*

Liquid crystalline dendrimers (LCDr) open up many possibilities for interesting molecular design. Liquid crystallinity can be induced by incorporating mesogenic groups into the body of the dendrimer, which can lead to the formation of calamitic nematic and smectic thermotropic phases [167]. An alternative strategy involves the bonding of mesogenic groups to the 'surface' of a dendrimer [168]. Here, formation of a liquid crystal would require a major rearrangement of structure. For example, in carbosilane LCDrs it has been suggested that dendrimer molecules, which appear spherical in structure, must rearrange internally to form either rods or discs in order that liquid crystalline phases can form [169]. Rods can then lead to the formation of a smectic-A phase and discs can self-assemble into columns, leading to the formation of a columnar phase.

The coarse-grained model of equation (27) was adopted for the first literature simulation of a liquid crystal dendrimer [170]. The model used was based on a carbosilane dendrimer, as shown in figure 15, in which the heavy atoms were represented with Lennard-Jones sites and the liquid crystalline groups were represented by Gay–Berne particles.

Putting the model dendrimer into a liquid crystal solvent, represented by Gay–Berne particles, gives rise to interesting behaviour whereby the dendrimer spontaneously changes structure from a spherical shape, which is adopted in a liquid, to a rod-shape (as shown in figure 16). Here the chains coupling the mesogens to the dendrimer core are able to rearrange so that the mesogens are able to align with the nematic

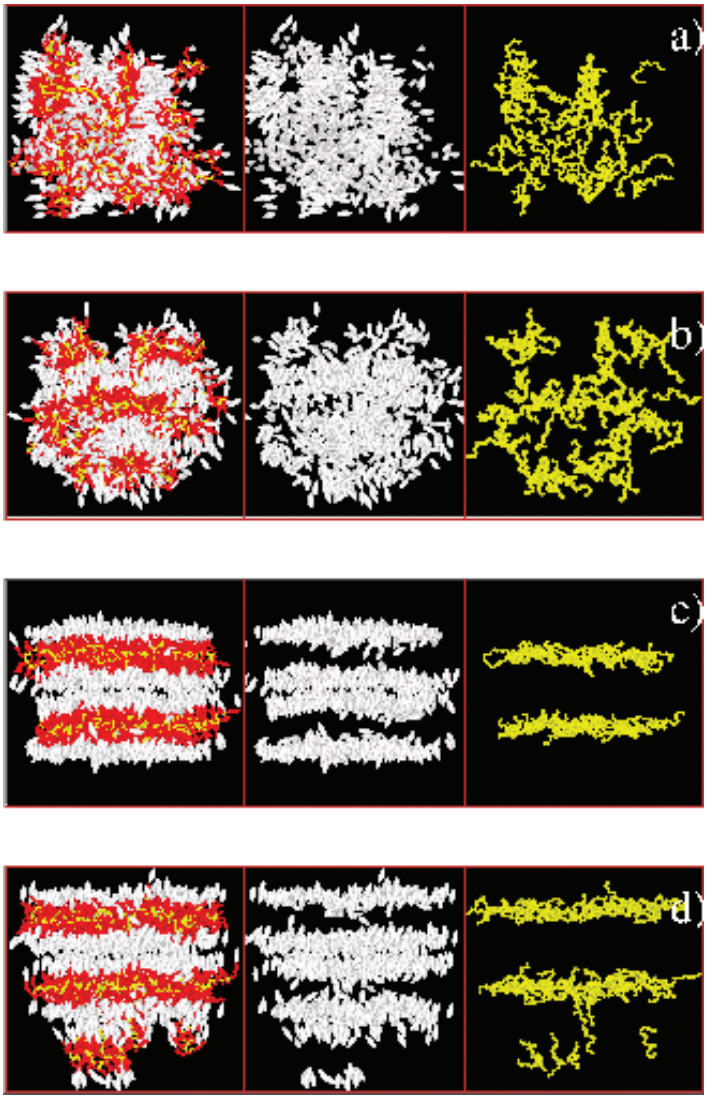

Figure 14. Snapshots showing the separate parts of SCLCP molecules from a coarse-grained simulation in the presence of an external potential of form, $E_{\text{external}} = -\epsilon^{\text{field}}\hat{u}_z^2$, mimicking a magnetic field. Yellow – polymer backbone. White – mesogenic units. Red – flexible spacer. (a) $\epsilon^{\text{field}} = 0.0 \times 10^{-20}$ J after 38 ns annealing run at 350 K. (b) $\epsilon^{\text{field}} = 0.2 \times 10^{-20}$ J from original cooling run after 6 ns at 350 K. (c) $\epsilon^{\text{field}} = 0.2 \times 10^{-20}$ J after further 38 ns of annealing at 350 K. (d) $\epsilon^{\text{field}} = 0.5 \times 10^{-20}$ J from original cooling run after 6 ns at 350 K. Reproduced from reference [156] with permission from the American Institute of Physics.

field of the solvent. It is suggested that this is the mechanism which mediates the formation of a liquid crystal in the bulk dendrimer. To examine this, the distribution functions from the dendrimer/solvent simulations can be used to help design a simpler coarse-grained model, shown in figure 17, which is sufficiently simple to allow the study

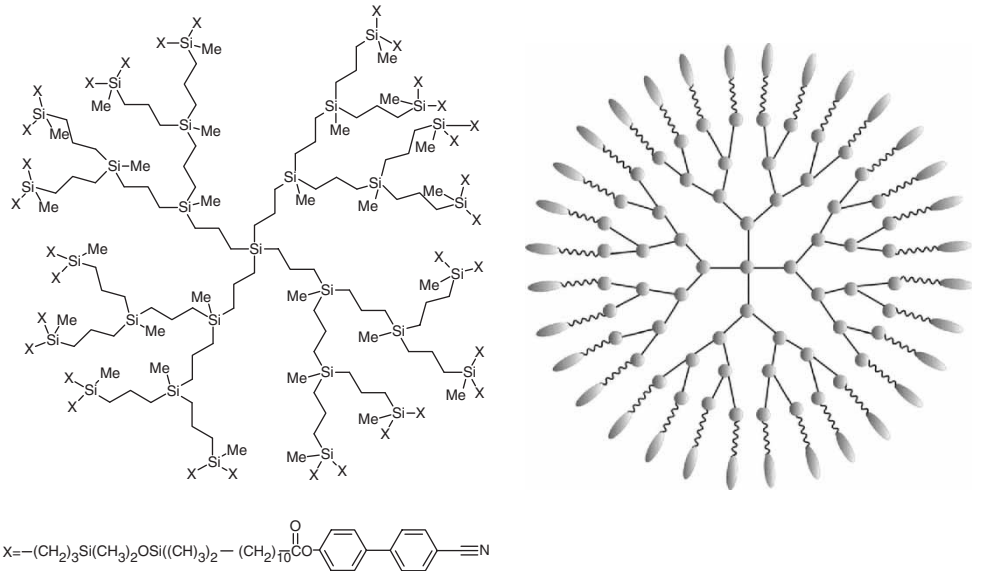

Figure 15. Chemical structure of a third generation carbosilane dendrimer studied in reference [170]. Left: chemical structure of the dendrimer. (The cyanobiphenyl group and the first part of the attached ester, including the carbonyl carbon, act as a fairly rigid mesogenic group within the dendrimer.) Right: schematic two-dimensional picture showing the branching points in the dendrimer leading to 32 terminal mesogenic groups.

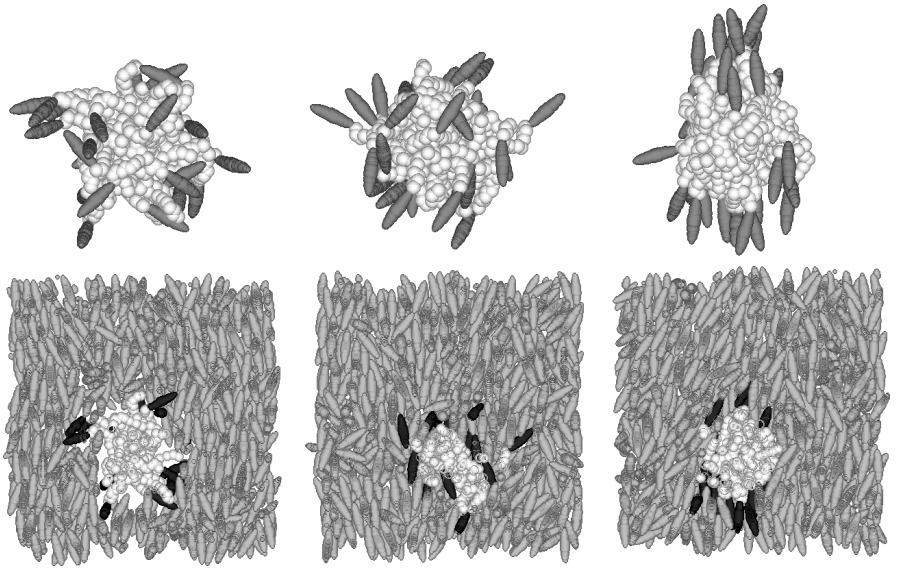

Figure 16. Configurations from a series of three time frames (left to right) showing the shape transition from sphere to rod in a third generation liquid crystal dendrimer placed in a nematic solvent. Top frames show the dendrimer with solvent removed. Reproduced from reference [170] with permission from the American Institute of Physics.

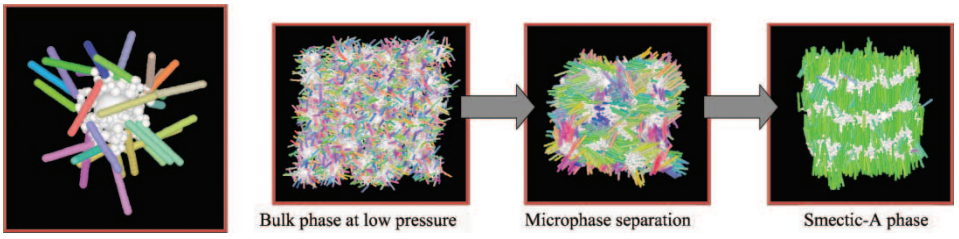

Figure 17. Left: a coarse-grained model for a third generation carbosilane dendrimer. Right: snapshots from three state-points at increasing density, showing from left-to-right: an isotropic phase, microphase separation into mesogen-rich and non-mesogen-rich domains and a smectic-A phase. Drawn from simulation results of a coarse grained model in reference [171, 172].

of bulk phases [171]. In figure 17, the mesogens are represented by soft repulsive spherocylinders [132], and the chains and core have been coarse-grained by the use of repulsive Lennard-Jones sites. In soft repulsive models, mesophase formation occurs as density is increased. In preliminary results from this model [171], increasing density leads to microphase separation into liquid crystal domains, which reorganize to form a smectic layer morphology with the core of the dendrimer sandwiched in the centre of the smectic layer (figure 17).

7. Some perspectives on the future

The rapid pace of computer development over the last decade has revolutionalized the simulation of liquid crystalline materials. At the atomistic level, it is now possible to get good descriptions of low molecular weight nematic materials and make reasonable predictions of key material properties (see section 4). One likely development in this area will take advantage of improved parallelization techniques to increase system sizes to thousands of molecules, which may be sufficient to extract good results for properties such as elastic constants that require larger system sizes than currently available.

It should be noted that in related fields, such as polymer simulation, the last few years have seen considerable success in linking modelling studies across the length scales. The same level of progress has not been seen for liquid crystal systems. While the quantum to atomistic route seems well founded (see section 4.1), the atomistic to mesoscale route seems to be less well developed. Some of the most successful liquid crystal models, Gay–Berne systems and spherocylinders, are in the mesoscale regime, but the phase diagrams calculated for these systems are not always helpful in studying thermotropic systems. In particular, the large density change at the phase transition between a liquid and a liquid crystal seen in such systems does not normally occur for thermotropics. So there is much work needed to generate models which can provide more faithful representations of phase behaviour. If this can be achieved, it should be much easier to move from atomistic to mesoscale by fitting to atomistic data. Hence, it will be possible to use mesoscale models in a more predictive way, i.e. to explore the

relationship between structure and bulk phase behaviour and predict how changes in structure can be used to engineer material properties.

One of the most interesting developments in liquid crystals arises from the synthesis of new classes of polyphilic molecules. In polyphilic systems, it is possible to engineer molecules to have different interaction regions, e.g. aliphatic, aromatic, fluoro, siloxane, and/or to incorporate a mixture of rigid liquid crystalline units and other flexible constituent parts into the molecule. For simple diblock copolymers this process is well understood and leads to self-assembly of regions containing similar interaction sites, giving rise to a rich phase diagram. However, for more complicated molecules, with many different competing interactions, self-assembly is more complex. Preliminary synthetic work has indicated that this strategy can provide a route to engineering new functional materials to act as biological mimics [12] and as new photonic materials [11]. Here, the key is controlling self-assembly to produce well-defined materials that are ordered at the nanoscale. For simulation, a real challenge is presented by this area. It would be highly desirable if simulation could be used as an engineering tool to help design new polyphilic liquid crystalline systems with the desired nanoscale structure for (say) a molecular electronics application. To this end, the progress made in coarse-grained simulation models for liquid crystals (section 6) and similar work for polymers chains [173–176] could point the way forward.

Acknowledgements

The author wishes to thank the UK research council, EPSRC, for supporting his work through research grants and DTA studentships. The author gratefully acknowledges the contributions from Dr. David Cheung, Dr. David Earl, Dr. Lorna Stimson, Dr. Melanie Cook, Dr. Carl McBride, Dr. Alejandro Cuetos and Mr. Zak Hughes to the author's own research in the area covered by this review. Discussions with Prof. M. P. Allen, Dr. A. J. Masters and Prof. F. Schmid are gratefully acknowledged.

References

[1] M. Schadt, Annu. Rev. Mater. Sci. **27,** 305 (1997).
[2] G. Strangi, V. Barna, R. Caputo, A. De Luca, C. Versace, N. Scaramuzza, C. Umeton, R. Bartolino, and G. N. Price, Phys. Rev. Lett. **94,** 063903 (2005).
[3] A. Chanishvili, G. Chilaya, G. Petriashvili, R. Barberi, R. Bartolino, G. Cipparrone, A. Mazzulla, and L. Oriol, Advan. Mater. **16,** 791 (2004).
[4] V. I. Kopp, Z. Q. Zhang, and A. Z. Genack, Prog. Quantum Electron. **27,** 369 (2003).
[5] D. J. Broer, J. A. M. M. van Haaren, P. van de Witte, and C. Bastiaansen, Macromol. Symposia **154,** 1 (2000).
[6] H. Kikuchi, M. Yokota, Y. Hisakado, H. Yang, and T. Kajiyama, Nat. Mater. **1,** 64 (2002).
[7] J. Gourlay, G. D. Love, P. M. Birch, R. M. Sharples, and A. Purvis, Opt. Commun. **137,** 17 (1997).
[8] G. D. Love, Appl. Opt. **36,** 1517 (1997).
[9] T. D. Wilkinson, W. A. Crossland, and A. B. Davey, Mol. Cryst. Liquid Cryst. **401,** 171 (2003).
[10] T. D. Wilkinson, W. A. Crossland, and A. B. Davey, Ferroelectrics **278,** 799 (2002).
[11] V. Percec, M. Glodde, T. K. Bera, Y. Miura, I. Shiyanovskaya, K. D. Singer, V. S. K. Balagurusamy, P. A. Heiney, I. Schnell, A. Rapp, H. W. Spiess, S. D. Hudson, and H. Duan, Nature **419,** 384 (2002).

[12] V. Percec, A. E. Dulcey, V. S. K. Balagurusamy, Y. Miura, J. Smidrkal, M. Peterca, S. Nummelin, U. Edlund, S. D. Hudson, P. A. Heiney, D. A. Hu, S. N. Magonov, and S. A. Vinogradov, Nature **430,** 764 (2004).
[13] W. Maier and A. Saupe, Zeitschrift Naturforschung **13a**, 564 (1958).
[14] L. Onsager, Annals New York Acad. Sci. **51,** 627 (1949).
[15] P. A. Lebwohl and G. Lasher, Phys. Rev. A **6,** 426 (1972).
[16] M. P. Neal and A. J. Parker, Chem. Phys. Lett. **294,** 277 (1998).
[17] T. Z. Qian and P. Sheng, Phys. Rev. E **58,** 7475 (1998).
[18] D. Svensek and S. Zumer, Phys. Rev. E **66,** 021712 (2002).
[19] G. Toth, C. Denniston, and J. M. Yeomans, Phys. Rev. E **67,** 051705 (2003).
[20] C. Denniston, G. Toth, and J. M. Yeomans, J. Statist. Phys. **107,** 187 (2002).
[21] S. V. Lishchuk, C. M. Care, and I. Halliday, J. Phys.-condens. matter **16,** S1931 (2004).
[22] C. M. Care, I. Halliday, K. Good, and S. V. Lishchuk, Phys. Rev. E **67,** 061703 (2003).
[23] A. Dupuis, D. Marenduzzo, and J. M. Yeomans, Phys. Rev. E **71,** 011703 (2005).
[24] J. B. Davies, S. Day, F. DiPasquale, and F. A. Fernandez, Electron. Lett. **32,** 582 (1996).
[25] S. Day and F. A. Fernandez. *Physical Properties of Liquid Crystal Nematics*, Chapter 12.5 (INSPEC, Institution of Electrical Engineers, London, 2001), pp. 652–657.
[26] C. M. Care and D. J. Cleaver, Rep. Prog. Phys. **68,** 2665 (2005).
[27] C. Chiccoli, P. Pasini, A. Sarlah, C. Zannoni, and S. Zumer, Phys. Rev. E **67,** 050703.1 (2003).
[28] D. Frenkel and B. M. Mulder, Mol. Phys. **55,** 1171 (1985).
[29] J. Talbot, D. Kivelson, M. P. Allen, G. T. Evans, and D. Frenkel, J. Chem. Phys. **92,** 3048 (1990).
[30] M. P. Allen, Phys. Rev. Lett. **65,** 2881 (1990).
[31] P. Bereolos, J. Talbot, M. P. Allen, and G. T. Evans, J. Chem. Phys. **99,** 6087 (1993).
[32] M. P. Allen and C. P. Mason, Molec. Phys. **86,** 467 (1995).
[33] P. J. Camp, C. P. Mason, M. P. Allen, A. A. Khare, and D. A. Kofke, J. Chem. Phys. **105,** 2837 (1996).
[34] D. Frenkel, H. N. W. Lekkerkerker, and A. Stroobants, Nature **332,** 822 (1988).
[35] S. C. McGrother, D. C. Williamson, and G. Jackson, J. Chem. Phys. **104,** 6755 (1996).
[36] P. K. Maiti, Y. Lansac, M. A. Glaser, and N. A. Clark, Phys. Rev. Lett. **92,** 025501 (2004).
[37] M. P. Allen and M. R. Wilson, J. Computer-Aided Molec. Design **3,** 335 (1989).
[38] M. A. Bates, in *Physical Properties of Liquid Crystal Nematics*, edited by D. Dunmar (INSPEC, London, 2001).
[39] J. G. Gay and B. J. Berne, J. Chem. Phys. **74,** 3316 (1981).
[40] L. F. Rull, Physica A **220,** 113 (1995).
[41] E. de Miguel, E. M. del Rio, J. T. Brown, and M. P. Allen, J. Chem. Phys. **105,** 4234 (1996).
[42] G. R. Luckhurst, R. A. Stephens, and R. W. Phippen, Liq. Cryst. **8,** 451 (1990).
[43] R. Berardi, A. P. J. Emerson, and C. Zannoni, Faraday Trans. **89,** 4069 (1993).
[44] C. Zannoni, J. Mater. Chem. **11,** 2637 (2001).
[45] E. de Miguel, Mol. Phys. **100,** 2449 (2002).
[46] A. Cuetos, J. M. Ilnytskyi, and M. R. Wilson, Molec. Phys. **100,** 3839 (2002).
[47] J. T. Brown, M. P. Allen, E. M. del Rio, and E. de Miguel, Phys. Rev. E **57,** 6685 (1998).
[48] M. A. Bates and G. R. Luckhurst, J. Chem. Phys. **104,** 6696 (1996).
[49] R. Berardi and C. Zannoni, J. Chem. Phys. **113,** 5971 (2000).
[50] J. T. Brown, PhD thesis, University of Bristol (1996).
[51] G. Luckhurst and P. Simmonds, Mol. Phys. **80,** 233 (1993).
[52] R. Berardi, S. Orlandi, and C. Zannoni, Chem. Phys. Lett. **261,** 357 (1996).
[53] M. A. Bates and G. R. Luckhurst, in *Structure and Bonding: Liquid Crystals*, edited by X. Peng and D.M.P. Mingos (Springer-Verlag, Heidelberg, 1999).
[54] D. Andrienko and M. P. Allen, Phys. Rev. E **65,** 021704 (2002).
[55] F. Barmes and D. J. Cleaver, Phys. Rev. E **69,** 061705 (2004).
[56] A. Chrzanowska, P. I. C. Teixeira, H. Ehrentraut, and D. J. Cleaver, J. Phys.-condens. Matter **13,** 4715 (2001).
[57] M. P. Allen, Mol. Phys. **96,** 1391 (1999).
[58] M. Al-Barwani and M. P. Allen, Phys. Rev. E **62,** 6706 (2000).
[59] M. P. Allen, J. Chem. Phys. **112,** 5447 (2000).
[60] N. Akino, F. Schmid, and M. P. Allen, Phys. Rev. E **63,** 041706 (2001).
[61] A. J. McDonald, M. P. Allen, and F. Schmid, Phys. Rev. E **63,** 010701 (2001).
[62] M. R. Wilson, in *Structure and Bonding: Liquid Crystals*, edited by M. Mingos (Springer-Verlag, Heidelberg, 1999), Vol. 94.
[63] M. R. Wilson, in *Handbook of Liquid Crystals*, D. edited by Demus, J. Goodby, G. W. Gray, H.-W. Spiess and V. Vill (Wiley-VCH, Weinheim, 1998), Vol. 1, Chapter III.3.
[64] D. L. G. Cheung. PhD thesis, University of Durham (2002).

[65] D. L. Cheung, S. J. Clark, and M. R. Wilson, Phys. Rev. E **65,** 051709 (2002).
[66] R. J. Woods, M. Khalil, W. Pell, S. H. Moffat, and V. H. Smith, J. Comput. Chem. **11,** 297 (1990).
[67] L. E. Chirlian and M. M. Francl, J. Comput. Chem. **8,** 894 (1987).
[68] C. M. Breneman and K. B. Wiberg, J. Comput. Chem. **11,** 361 (1990).
[69] W. Jorgensen, D. Maxwell, and J. TiradoRives, J. Am. Chem. Soc. **118,** 11225 (1996).
[70] W. Jorgensen and J. TiradoRives, J. Am. Chem. Soc. **110,** 1657 (1988).
[71] G. A. Kaminski, J. Phys. Chem. B **109,** 5884 (2005).
[72] S. Patel and C. L. Brooks, J. Comp. Chem. **25,** 1 (2004).
[73] S. Patel, A. D. Mackerell, and C. L. Brooks, J. Comp. Chem. **25,** 1504 (2004).
[74] G. Lamoureux and B. Roux, J. Chem. Phys. **119,** 3025 (2003).
[75] S. Y. Noskov, G. Lamoureux, and B. Roux, J. Phys. Chem. B **109,** 6705 (2005).
[76] D. J. Willock, S. L. Price, M. Leslie, and C. R. A. Catlow, J. Comput. Chem. **16,** 628 (1995).
[77] R. Berardi, L. Muccioli, S. Orlandi, M. Ricci, and C. Zannoni, Chem. Phys. Lett. **389,** 373 (2004).
[78] D. L. Cheung, S. J. Clark, and M. R. Wilson, J. Chem. Phys. **121,** 9131 (2004).
[79] C. McBride, M. R. Wilson, and J. A. K. Howard, Molec. Phys. **93,** 955 (1998).
[80] C. McBride, PhD thesis, University of Durham (1999).
[81] R. Berardi, L. Muccioli, and C. Zannoni, ChemPhysChem. **5,** 104 (2004).
[82] M. R. Wilson and M. P. Allen, Mol. Cryst. Liq. Cryst. **198,** 465 (1991).
[83] M. R. Wilson and M. P. Allen, Liq. Cryst. **12,** 157 (1992).
[84] J. W. Emsley, G. R. Luckhurst, and C. P. Stockley, Proc. R. Soc. Lond. A **381,** 117 (1982).
[85] C. W. Cross and B. Fung, J. Chem. Phys. **101,** 6839 (1994).
[86] M. R. Wilson, J. Chem. Phys. **107,** 8654 (1997).
[87] M. P. Allen and A. J. Masters, J. Mater. Chem. **11,** 2678 (2001).
[88] F. C. Frank, Discuss. Faraday Soc. **25,** 19 (1958).
[89] D. J. Cleaver and M. P. Allen, Phys. Rev. A **43,** 1918 (1991).
[90] M. P. Allen, M. A. Warren, M. R. Wilson, A. Sauron, and W. Smith, J. Chem. Phys. **105,** 2850 (1996).
[91] N. H. Phuong, G. Germano, and F. Schmid, J. Chem. Phys. **115,** 7227 (2001).
[92] N. H. Phuong and F. Schmid, J. Chem. Phys. **119,** 1214 (2003).
[93] A. Poniewierski and J. Stecki, Molec. Phys. **38,** 1931 (1979).
[94] G. Germano, M. P. Allen, and A. J. Masters, J. Chem. Phys. **116,** 9422 (2002).
[95] G. R. Luckhurst and K. Satoh, Mol. Cryst. Liquid Cryst. **402,** 321 (2003).
[96] H. Steuer and S. Hess, Phys. Rev. Lett. **94,** 027802 (2005).
[97] S. Sarman and D. J. Evans, J. Chem. Phys. **99,** 9021 (1993).
[98] S. Sarman, J. Chem. Phys. **103,** 10378 (1995).
[99] A. M. Smondyrev, G. B. Loriot, and R. A. Pelcovits, Phys. Rev. Lett. **75,** 2340 (1995).
[100] S. Cozzini, L. F. Rull, G. Ciccotti, and G. V. Paolini, Physica A **240,** 173 (1997).
[101] D. L. Cheung, S. J. Clark, and M. R. Wilson, Chem. Phys. Lett. **356,** 140 (2002).
[102] U. Finkenzeller, T. Geelhaar, G. Weber, and L. Pohl, Liq. Cryst. **5,** 313 (1989).
[103] A. V. Zakharov, A. V. Komolkin, and A. Maliniak, Phys. Rev. E **59,** 6802 (1999).
[104] A. V. Zakharov and R. Y. Dong, Phys. Rev. E **63,** 011704 (2001).
[105] S. Kuwajima and A. Manabe, Chem. Phys. Lett. **332,** 105 (2000).
[106] M. C. W. van Boxtel, R. H. C. Janssen, C. W. M. Bastiaansen, and D. J. Broer, J. App. Phys. **89,** 838 (2001).
[107] M. Schadt, H. Seiberle, and A. Schuster, Nature **381,** 6579 (1996).
[108] P. van de Witte, E. E. Neuteboom, M. Brehmer, and J. Lub, J. Appl. Phys. **85,** 7517 (1999).
[109] A. Ferrarini, G. J. Moro, and P. L. Nordio, Liq. Cryst. **19,** 397 (1995).
[110] L. Feltre, A. Ferrarini, F. Pacchiele, and P. L. Nordio, Mol. Cryst. Liq. Cryst. **290,** 109 (1996).
[111] A. di Matteo, S. M. Todd, G. Gottarelli, G. Solladie, V. E. Williams, R. P. Lemieux, F. A., and G. P. Spada, J. Am. Chem. Soc. **123,** 7842 (2001).
[112] A. Ferrarini, G. Gottarelli, P. L. Nordio, and G. P. Spada, J. Chem. Soc. Perkin Trans. 2, 411 (1999).
[113] A. Ferrarini and P. L. Nordio, J. Chem. Soc. Perkin Trans. 2, 455 (1998).
[114] A. Ferrarini, P. L. Nordio, P. V. Shibaev, and V. P. Shibaev, Liq. Cryst. **24,** 219 (1998).
[115] A. Ferrarini, G. J. Moro, and P. L. Nordio, Molec. Phys. **87,** 485 (1996).
[116] A. Ferrarini, G. J. Moro, and P. L. Nordio, Phys. Rev. E **53,** 681 (1996).
[117] D. J. Earl and M. R. Wilson, J. Chem. Phys. **120,** 9679 (2004).
[118] G. Gottarelli, M. Hibert, B. Samori, G. Solladir, G. P. Spada, and R. Zimmermann, J. Am. Chem. Soc. **105,** 7318 (1983).
[119] G. Gottarelli, G. Proni, G. P. Spada, D. Fabbri, S. Gladiali, and C. Rosini, J. Org. Chem. **61,** 2013 (1996).
[120] M. Solymosi, R. J. Low, M. Grayson, M. P. Neal, M. R. Wilson, and D. J. Earl, Ferroelectrics **277,** 483 (2002).

[121] M. P. Neal, M. Solymosi, M. R. Wilson, and D. J. Earl, J. Chem. Phys. **119,** 3567 (2003).
[122] M. Osipov and H. Kuball, Eur. Phys. J. E **5,** 589 (2001).
[123] D. J. Earl, PhD thesis, University of Durham (2003).
[124] H. Kamberaj, M. A. Osipov, R. J. Low, and M. P. Neal, Mol. Phys. **102,** 431 (2004).
[125] D. J. Earl and M. R. Wilson, J. Chem. Phys. **119,** 10280 (2003).
[126] A. J. Slaney, I. Nishiyama, P. Styring, and J. W. Goodby, J. Mater. Chem. **2,** 805 (1992).
[127] M. J. Watson, M. K. Horsburgh, J. W. Goodby, K. Takatoh, A. J. Slaney, J. S. Patel, and P. Styring, J. Mater. Chem. **8,** 1963 (1998).
[128] J. Thisayukta, H. Niwano, H. Takezoe, and J. Watanabe, J. Am. Chem. Soc. **124,** 3354 (2002).
[129] D. J. Earl, M. A. Osipov, H. Takezoe, Y. Takanishi, and M. R. Wilson, Phys. Rev. E **71,** 021706 (2005).
[130] M. P. Allen, Phys. Rev. E **47,** 4611 (1993).
[131] M. J. Cook and M. R. Wilson, J. Chem. Phys. **112,** 1560 (2000).
[132] M. R. Wilson and D. J. Earl, J. Mater. Chem. **11,** 2672 (2001).
[133] M. R. Wilson, J. Chem. Phys. **107,** 8654 (1997).
[134] C. McBride and M. R. Wilson, Molec. Phys. **97,** 511 (1999).
[135] D. J. Earl, J. Ilnytskyi, and M. R. Wilson, Molec. Phys. **99,** 1719 (2001).
[136] M. Wilson, in *Advances in the Computer Simulations of Liquid Crystals*, edited by P. Pasini and C. Zannoni (Kluwer Academic Publishers, Dordrecht, 2000), Chapter 13, pp. 389–412.
[137] J. M. Ilnytskyi and M. R. Wilson, Comput. Phys. Commun. **148,** 43 (2002).
[138] J. C. Shelley, M. Y. Shelley, R. C. Reeder, S. Bandyopadhyay, and M. L. Klein, J. Phys. Chem. B **105,** 4464 (2001).
[139] L. Whitehead, C. M. Edge, and J. W. Essex, J. Comput. Chem. **22,** 1622 (2001).
[140] L. Saiz and M. L. Klein, Account. Chem. Res. **35,** 482 (2002).
[141] V. Knecht, S. J. Marrink, and A. E. Mark, Biophys. J. **88,** 384A (2005).
[142] A. H. de Vries, A. E. Mark, and S. J. Marrink, J. Am. Chem. Soc. **126,** 4488 (2004).
[143] S. J. Marrink, A. H. de Vries, and A. E. Mark, J. Phys. Chem. B **108,** 750 (2004).
[144] A. H. de Vries, S. Yefimov, A. E. Mark, and S. J. Marrink, P. Nat. Acad. Sci. USA **102**, 5392 (2005).
[145] S. J. Marrink, J. Risselada, and A. E. Mark, Chem. Phys. Lipids **135,** 223 (2005).
[146] F. Goujon, P. Malfreyt, and D. J. Tildesley, Mol. Phys. **103,** 2675 (2005).
[147] P. Malfreyt and D. J. Tildesley, Langmuir **16,** 4732 (2000).
[148] A. AlSunaidi, W. K. Den Otter, and J. H. R. Clarke, Phil. Trans. Roy. Soc. London A **362,** 1773 (2004).
[149] P. Espanol and P. Warren, Europhys. Lett. **30,** 191 (1995).
[150] R. D. Groot and P. B. Warren, J. Chem. Phys. **107,** 4423 (1997).
[151] Y. K. Levine, A. E. Gomes, A. F. Martins, and A. Polimeno, J. Chem. Phys. **122,** 144902 (2005).
[152] A. E. Gomes, A. F. Martins, and A. Polimeno, Molec. Crys. Liq. Cryst. **435,** 795 (2005).
[153] H. Ringsdorf and A. Schneller, British Polym. J. **13,** 43 (1981).
[154] H. Finkelmann, H. Ringsdorf, and J. Wendorff, Makromol. Chem. **179,** 273 (1978).
[155] A. V. Lyulin, M. S. Al-Barwani, M. P. Allen, M. R. Wilson, I. Neelov, and N. K. Allsopp, Macromolecules **31,** 4626 (1998).
[156] L. M. Stimson and M. R. Wilson, J. Chem. Phys. **123,** 034908 (2005).
[157] P. Davidson and A. M. Levelut, Liq. Cryst. **11,** 469 (1992).
[158] L. Noirez, Europhys. Lett. **46,** 728 (1999).
[159] S. Lecommandoux, L. Noirez, M. F. Achard, and F. Hardouin, Macromolecules **33,** 67 (2000).
[160] I. W. Hamley, J. P. A. Fairclough, S. M. King, J. S. Pedersen, R. M. Richardson, C. T. Imrie, and A. A. Craig, Liq. Cryst. **22,** 679 (1997).
[161] R. M. Richardson, E. B. Barmatov, I. J. Whitehouse, V. P. Shibaev, T. Yongjie, and M. H. F. Godhino, Mol. Cryst. Liq. Cryst. **330,** 285 (1999).
[162] S. Lecommandoux, L. Noirez, M. F. Achard, and F. Hardouin, J. Phys. II **7,** 1417 (1997).
[163] S. J. Picken, L. Noirez, and G. R. Luckhurst, J. Chem. Phys. **109,** 7612 (1998).
[164] P. Davidson, L. Noirez, J. P. Cotton, and P. Keller, Liq. Cryst. **10,** 111 (1991).
[165] L. Noirez, P. Keller, and J. P. Cotton, Liq. Cryst. **18,** 129 (1995).
[166] S. Lecommandoux, L. Noirez, H. Richard, M. F. Achard, C. Strazielle, and F. Hardouin, J. Phys. II **6,** 225 (1996).
[167] V. Percec, P. W. Chu, G. Ungar, and J. P. Zhou, J. Am. Chem. Soc. **117,** 11441 (1995).
[168] R. M. Richardson, S. A. Ponomarenko, N. I. Boiko, and V. P. Shibaev, Liq. Cryst. **26,** 101 (1999).
[169] S. A. Ponomarenko, N. I. Boiko, V. P. Shibaev, R. M. Richardson, I. J. Whitehouse, E. A. Rebrov, and A. M. Muzafarov, Macromolecules **33,** 5549 (2000).
[170] M. R. Wilson, J. M. Ilnytskyi, and L. M. Stimson, J. Chem. Phys. **119,** 3509 (2003).

[171] L. M. Stimson, PhD thesis, University of Durham (2003).
[172] Z. E. Hughes, M. R. Wilson, and L. M. Stimson, Soft Matter, in press (2005), DOI: 10.1039/6300001a.
[173] W. Tschop, K. Kremer, J. Batoulis, T. Burger, and O. Hahn, Acta Polym. **49,** 61 (1998).
[174] H. Meyer, O. Biermann, R. Faller, D. Reith, and F. Muller-Plathe, J. Chem. Phys. **113,** 6264 (2000).
[175] R. Faller, Polymer **45,** 3869 (2004).
[176] R. Faller and F. Muller-Plathe, Polymer **43,** 621 (2002).